THERMAL SHOCK RESISTANCE OF CERAMICS

by

ROBERT STEVEN GOODOF

Submitted in partial fulfillment of the requirements

for the degrees of

MASTER OF SCIENCE IN MATERIALS SCIENCE

and

BACHELOR OF SCIENCE, METALLURGY AND MATERIALS SCIENCE

at the

Massachusetts Institute of Technology

June 1973

Signature of Author ..... Signature redacted .....
Department of Metallurgy and Materials Science
May 11, 1973

Certified by ..... Signature redacted .....
Thesis Supervisor

Accepted by ..... Signature redacted .....
Chairman, Departmental Committee on Graduate Students

ABSTRACT

THERMAL SHOCK RESISTANCE OF CERAMICS

by

ROBERT STEVEN GOODOF

Submitted to the Department of Metallurgy and Materials Science on May 11, 1973, in partial fulfillment of the requirements for the degrees of Master of Science in Materials Science and Bachelor of Science in Metallurgy and Materials Science.

The present investigation into the thermal shock resistance of ceramics was concentrated on the effect of certain properties on resistance to damage from thermal cycling. The reliability and predictability of behavior based on thermal stress parameters and fracture energy criteria were brought to question, the former in the general case of the behavior of brittle materials, and the latter in the particular case where non-Griffith type flaws exist in the material.

Brick-shaped samples were dry pressed, fired, and then repeatedly quenched from 1000°C into an ice bath. Periodic removal for examination of brick and fracture surfaces was conducted, along with tests for surface fracture energy, strength, and modulus. Evaluation of data and use of determined properties to compare thermal shock parameters was conducted. Whereas it has been known that simple thermoelastic parameters do not always correctly predict gross material failure, it was also determined that fracture mechanical approaches (energy considerations) are not necessarily accurate in the case where blunted flaws predominate in the sample. The energy-based model does not appear to account for increased thermal shock damage resistance in the surface region of the bricks. This suggests that (a) an energy-based model be analyzed using blunt-tipped cracks and (b) an analysis be carried out which includes the immediate local applied stress state.

Excellent shock resistance was exhibited by alumina-titania bricks, due to the existence of short, blunt, shrinkage cracks in the material after sintering. Material properties such as strength and modulus seemed more dependent upon the particular fabrication and firing methods than upon the extent of shrinkage cracking. Alumina-9%magnesia and titania-3%silica were far inferior to the alumina-titania bricks in terms of resistance to damage by repeated thermal shocking. Stress-free (as-fired) alumina-titania exceeded the performance limits predicted by the theory, while the alumina-magnesia was not far from the predicted behavior.

Donald Robert Uhlmann
Associate Professor of Ceramics

TABLE OF CONTENTS

LIST OF FIGURES

LIST OF TABLES

ACKNOWLEDGMENTS

The author wishes to express his thanks to the Department of Interior, Office of Coal Research, for their sponsorship of this research project. Gratitude is also deserving by Professor D.R. Uhlmann for his advice and inspiration, and to the technicians of the Ceramics Department, particularly R.L. Stanton, for their valuable assistance during the course of my work.

I. INTRODUCTION

The very properties of refractory oxides which make them such capable insulators naturally appear to render these materials catastrophically susceptible to damage in thermal shock and thermal fatigue. Typically low thermal conductivities and thermal diffusivities cause highly nonuniform temperature gradients through thick parts, giving rise to thermal stresses which are only relieved when such gradients become linear. These stresses may readily become extensive and effect cracking and failure of improperly designed ceramic parts.

Proper design of parts expected to withstand severe temperature changes, whether singularly or repeatedly, requires the optimal combination of several different effects and properties of the ceramic system under consideration. These variables include average void size, void fraction, grain size, and composition. It is the attempt to discern the effect of such basic properties on thermal shock behavior that has led to this research. The goal is to prescribe methods of designing thermal fatigue-resistant ceramic bricks (for use in the preheater of a magneto-hydrodynamic power source) via examination of the phenomena interpreted as most important to such a design. Tests to determine relevant properties, i.e., surface fracture energy, relative tensile strengths, moduli, and crack densities, will be conducted to reach conclusions regarding material design for the most satisfactory system.

II. BACKGROUND

Two significant approaches to thermal shock analysis have been proffered and extensively studied on a theoretical basis. They are, generally, a) the solution to the thermoelastic equation for the state of stress in a part and b) the solution to the fixed-grip problem for crack growth, using energy considerations to determine the stability of a crack in a thermally shocked piece.

The first analysis is carried out by equating the overall stress state in the body to the general thermoelastic equation for stress.[1] For a thin plate under no external stresses (the only stresses in the body arise from thermal gradients), the stress, σ, is expressed by equation (1):

$$\sigma = \frac{\alpha E \Delta T}{(1-\nu)} \tag{1}$$

where α is the thermal expansion coefficient, E the Young's modulus, Δ T the difference between the temperature at the point of interest and the average temperature of the body, and ν is Poisson's ratio. By setting $\sigma = S_t$, the tensile strength of the material, the maximum temperature differential for material failure can be determined:

$$\Delta T_{max} = \frac{S_t (1-\nu)}{\alpha E} \tag{2}$$

where steady state heat flow is assumed. The difficulty of solving this equation for more complicated geometries, states

of external stress, and particular temperature distributions suggests that this simple expression be used as a parameter to relate the relative states of thermally induced stress in different materials of similar geometries. Hence:

$$R = \frac{S_t(1-\nu)}{\alpha E} \quad [2] \qquad (3)$$

where it is obvious that larger values of R indicate relatively greater permissible temperature variations before excessive stresses are incurred.

Simple extension of this parameter to relate to heat flow leads to another useful parameter of a similar nature:

$$k\Delta T = Q$$

$$R' = \frac{kS_t(1-\nu)}{\alpha E} \quad [2] \qquad (4)$$

which is a convenient measure of the maximum heat flux allowable in a part (Here k is the thermal conductivity of the material and Q is the heat flux). Further extension to unsteady state brings about equation (5) for a maximum rate of surface heating:

$$\kappa\Delta^2 T = \frac{\partial T}{\partial t}$$

$$R'' = \frac{\kappa S_t(1-\nu)}{\alpha E} \quad [2] \qquad (5)$$

where κ is the thermal diffusivity ($\kappa = \frac{k}{\rho C_p}$) of the material.

Here σ is the density and C_p is the heat capacity.

It would be expected that when any of the above parameters are reached and/or exceeded under thermal shock conditions, failure of the part would occur (assuming brittle failure). Such an assumption is reasonable, since the induced stresses would then have exceeded the tensile strength of the material. In fact, however, this does not always occur, mainly because the failure of a local volume and the subsequently nucleated crack do not necessarily cause the entire part to fail. The straightforward thermoelastic analysis results in a prediction for crack nucleation, but the difference between crack nucleation and failure of the part may be quite significant in terms of the number of thermal shock cycles or temperature differences experienced by specimens.

The analysis of the nucleated crack and subsequent thermal shocking (or the effect of initial flaws on a first shock cycle) was conducted by Hasselman[3, 4] using a fracture mechanics approach with fixed grip assumptions. His energy considerations led him to believe that under certain states of stress (or temperature gradients) small initially existent flaws may grow quasistatically (stably). The thermally stressed plate becomes, therefore, a direct analog of the fixed-grips fracture toughness test.[5]

More specifically, the relation between thermal strain and crack length (Figure 1) is determined, and follows equation (6):

$$\Delta T = \left[\frac{\pi G(1-\nu)}{2E_o\alpha^2(1-\nu)}\right]^{1/2}\left[1 + \frac{16(1-\nu^2)\ell^3 N}{9(1-2\nu)}\right]\left[\ell\right]^{-1/2} \qquad (6)$$

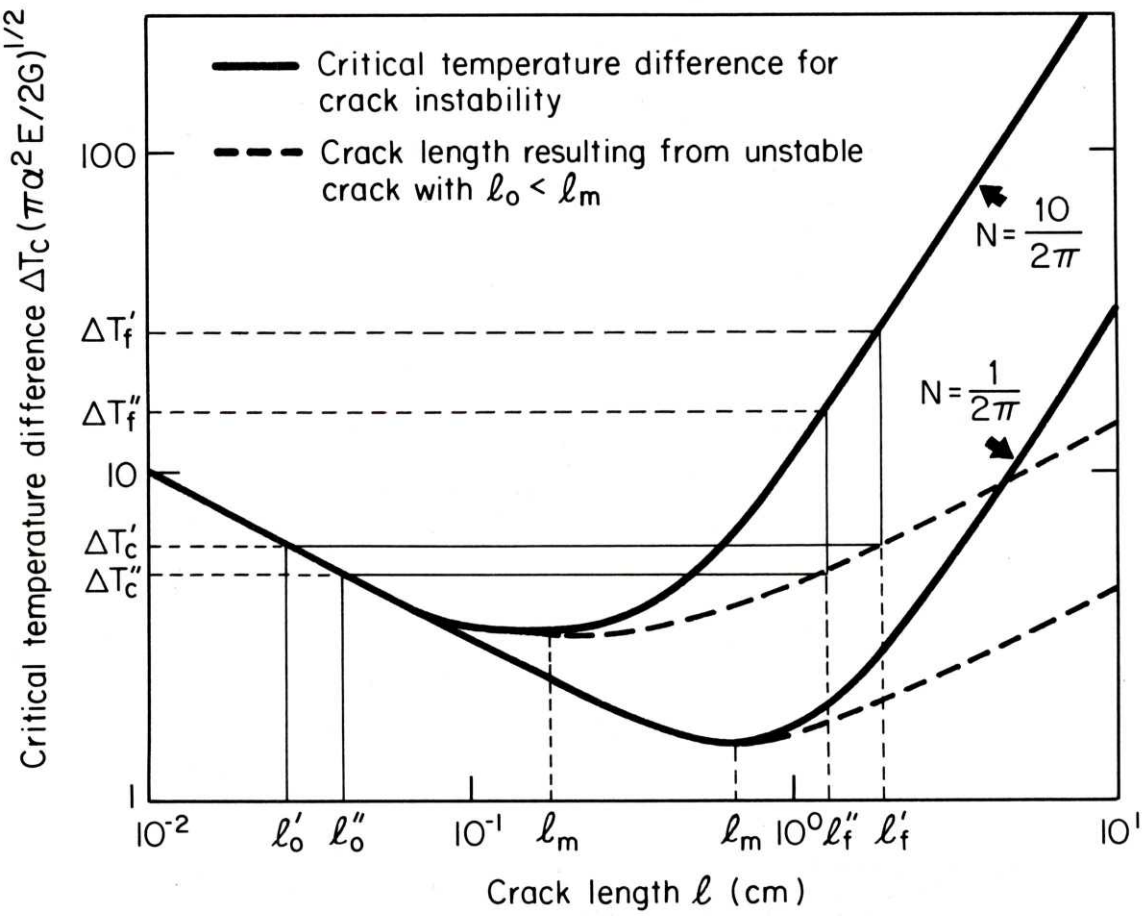

Figure 1. Stability-instability regions of crack growth.[3] $\Delta T_c'$ and $\Delta T_c''$ are the maximum ΔT (°C) for unstable crack growth for lengths ℓ_o' and ℓ_o''. ℓ_m is the maximum crack length for each curve which will permit unstable growth to a stable crack length (ℓ_m). It corresponds to the minimum in T to unstable propagation. $\Delta T_f'$ and $\Delta T_f''$ are the maximum ΔT's for further unstable crack growth after initial unstable propagaton, to lengths ℓ_f'' and ℓ_f'. Dotted lines identify crack lengths ℓ_f' and ℓ_f'' ($\geq \ell_m$) for stability for a given N and ℓ_o' and ℓ_o'', after unstable growth. Solid line is graph of Equation (6).

where G is the surface fracture energy, E_o the Young's modulus of the unflawed material, α the thermal expansion coefficient, N is the crack density, ℓ the instantaneous crack length, and ν is Poisson's ratio.[3]

This approach infers that, once a flaw of initial length has reached some particular stable length ℓ_f, sizable thermal strains (temperature differences) are required to bring about further unstable crack growth. Such temperature differences are larger than the parameter-estimated temperature differences, provided that the crack has propagated stably to ℓ_f. In fact, we see from Equation (4) that the higher the crack density N_ℓ (number of cracks per unit length), the larger the temperature difference required for further unstable propagation of any flaws.

As a fracture mechanical analogy, Hasselman proposed his own set of thermal shock damage resistance parameters:

$$R''' = \frac{E}{S_t^2(1-\nu)}^{[2]} \tag{7}$$

$$R'''' = \frac{GE}{S_t^2(1-\nu)}^{[2]} \tag{8}$$

Equation (7) represents the minimum elastic energy at fracture available for crack propagation of a given material; and equation (8) represents the minimum extent (distance) of crack propagation on the initiation of thermal stress fracture (growth distance of the first cracks under thermal shock conditions).

In other work, Hasselman[4] provided another parameter for predicting the mode of failure of a brittle piece, whether catastrophic or "controlled". Comparison of crack area to cross-sectional area provides the ability to predict the thermal shock behavior of the material in question. Equation (9) gives a value for the crack area:

$$A = \frac{4\pi b^3(1-\nu)}{7EGN} \qquad (9)$$

where b is a typical dimension of the sample. If this value is greater than the cross section, the piece will fail catastrophically; if less, then the piece will fail via a succession of thermal shock cycles and crack growths (stable propagation), the final cycle being the one where the value of Equation (9) exceeds the cross section area.

Thermal shock behavior would appear to depend on the continuity of the inspected material, if for no other reason than heat flow considerations. Early work by Schurecht[6] and Morgan[7] showed that maximum refractory performance was produced at porosity fractions between 15-28%. Thermal conductivity (k) has been shown to vary as Equation (10):

$$k = k_o(1-p)^n \quad [8] \qquad (10)$$

where p is the volume fraction of porosity. In the same investigation, Coble found other materials properties to relate to porosity fraction in the following manner:

$$E = E_o\exp(-Kp) \quad [8,9] \qquad (11)$$

$$\sigma = \sigma_o\exp(-6p) \quad [8] \qquad (12)$$

where Coble's K had the value 3.5, while other investigators found values ranging up to 4.5.[10] For two continuous phases, more nearly linear variations of E and σ (tensile strength) have been determined.[11] It is apparent, therefore, that certain properties are significantly affected by the void fraction of material.

Of possible concern is the effect of such pores and voids on mechanical stress states in the material. This effect was determined by Florence and Goodier:[12]

$$\sigma = k'\alpha E a \tau$$

where τ is the temperature gradient, a is the sphere radius, and k' is a constant. This expression is for the micromechanical stress around a void in a material subject to uniform heat conditions. This result is based on assumptions of plane stress and a hole of circular cross section. The case where k'= 1 applies to cylindrical holes. Similar types of stress concentration results have been obtained for holes in a plate and spherical cavities in a thick part.[13] The stresses arising from heat gradients are, in fact, equivalent to some externally applied mechanical stress, when the concentrating factor is considered. For small cavities, the surrounding heat flow field is uniform and stresses of the order of 4000 psi may easily arise (according to Equation (13)).[14]

These voids, however, may serve another purpose, that of blunting or arresting sharp cracks propagating through the part under thermal stresses. Modified Griffith criteria show that the

crack tip radius is an important parameter in the stress concentration effect of a flaw in a material, and so this manner of arresting cracks (by requiring more applied stress to give local failure) is theoretically inviting. Hasselman's energy-based analysis has led him to conclude that such flaws, inhomogeneities, voids, and second phase particles should be included in a material designed for optimal resistance to thermal shock damage.

Work on the effect of grain size on thermal shock damage resistance goes hand-in-hand with studies of the importance of initial strength on damage resistance. Hasselman[15] derived Equation (14), showing in the process that the fracture strength of the shocked material was inversely proportional to the initial strength of the part and proportional to the square root of the crack density:

$$S_f = \frac{GEN^{1/2}}{\pi S_o} \qquad (14)$$

where S_f is the fracture stress of the shocked material and S_o is the initial strength of the same material.

This generalization, coupled with the Hall-Petch relationship between grain size and strength (Equation 15):

$$\tau = \tau_o + Kd^{-1/2} \qquad (15)$$

where τ_o is a constant with units of stress, K is a constant, and d is the grain size, indicates that larger grain sizes reduce overall as-fired strength; and this would appear to resist more effectively unstable crack growth. Furthermore, Hasselman[15] showed consistently and experimentally how the strength of a given

material varied with the difference in quenching temperatures (Figure 2). Thus there is sufficient understanding that grain size affects the initial and post-quench strength of a material, and that the post-quench strength is also dependent upon the degree of the quench, as Figure 2 shows. Gupta[16] substantiated this generalization for alumina rods (Figure 3).

Other relevant aspects of thermal shock investigations include resistance to creep, chemical attack, and compressive strength. More work by Hasselman[17] showed that larger grains increase creep resistance by reducing grain boundary sliding. Since chemical attack occurs preferentially at grain boundaries, the overall increase of grain size should improve the resistance of a refractory to such attack (by reducing the total grain boundary surface area). The other noted property, compressive strength, is generally a more important service property in the use of refractory bricks than is the tensile strenth. Little in-depth analysis has been completed, but available data show that smaller grain sizes increase compressive strength[18] by providing arresting mechanism to failure by shear. Thus it appears that compromises must be made to effect a material with optimal service properties.

It is seen, therefore, that there are two main approaches to material design, where thermal shock is concerned. The first method attempts to maximize the resistance to crack nucleation by maximizing parameters R, R', and R". This can be done by using materials with high tensile strength and low Young's modulus and

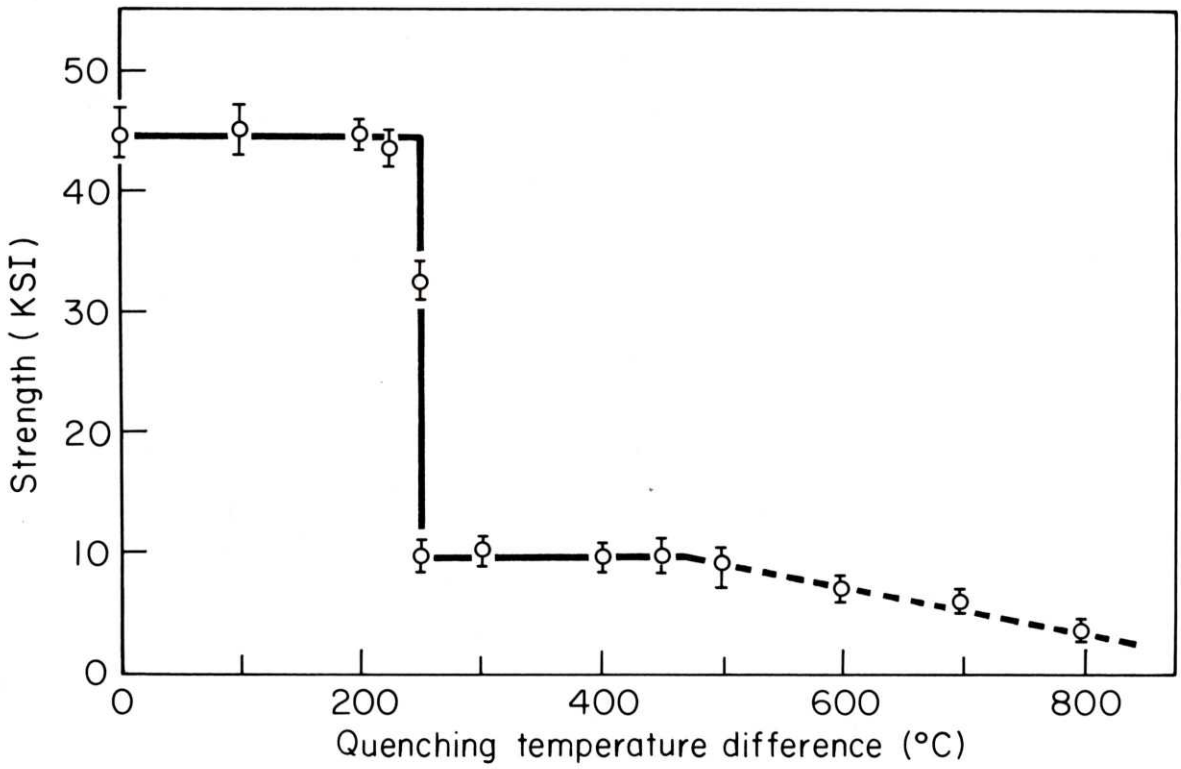

Figure 2. Typical post-quench strength-quench temperature plot for polycrystalline alumina (single quench).[15] The discontinuous drop in strength corresponds primarily to the value R (Equation 1).

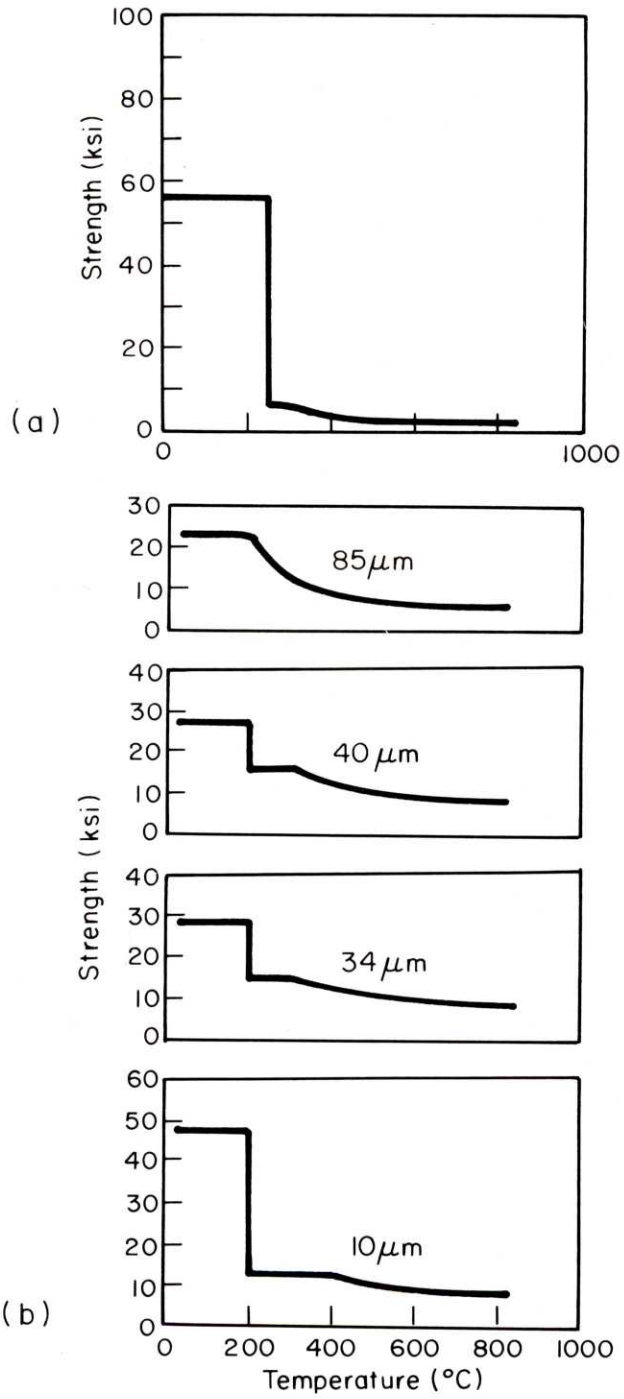

Figure 3. Post-quench strengths as function of quench temperature. (a) single crystal sapphire, (b) polycrystalline Al_2O_3 with noted average grain sizes.[16]

thermal expansion coefficients. High strengths demand relatively flaw-free materials. The second approach seeks to minimize unstable propagation of any and all small flaws initially present or formed by a first shocking cycle. In fact, the contention is based on a desire for a high initial crack density and seeks low strength materials with high Young's modulus and fracture surface energy. An analogy has been made between the two aforementioned approaches by application of Griffith theory[19] (see Appendix A). For a single crack in a plate, this analysis shows:

$$R \propto R''' \tag{16}$$

This implies that the two approaches are in theory the same. The real difference for our purposes is that the fracture mechanics analysis assumes (or desires) the presence of microcracks whose stability and size artificially raise the value of G, permitting local fractures, whereas the thermoelastic approach neglects the internal structure of the material and assumes that gross failure occurs when the tensile stress is reached at any point in the body.

III. EXPERIMENTAL PROCEDURE

A. General Approach

Hasselman's derivations and observations suggest that a few basic variable states may instill maximized resistance to thermal shock damage in a ceramic. The presence of inhomogeneities, voids, defects, plastic (energy absorbing) second phases, and the like may arrest cracks which would otherwise propagate unhindered through a dense, pure piece. In addition, since it has been shown and experimentally verified that a large size leads to increased post shock strength, specimens of greater average grain size may ensure further damage resistance. These inferences merit study for their actual effects on materials subjected to thermal shock conditions.

Samples to be fabricated and tested will be "injected" with voids, hopefully of sizes comparable to the grain size (or less) of the fired ceramic. This will be done by adding polyvinyl alcohol (PVA)[20] particles, which will vaporize during the firing process. The vaporization will leave numerous voids in the as-fired brick, hopefully to blunt the propagating cracks during conditions of thermal shocking.

The addition of inclusions and various energy absorbing second phases would increase the surface fracture energy of the material. However, the difficulty of adding a component which may satisfy this desire becomes apparent when one realizes that it must survive high firing temperatures and must be ductile in the range 800°-1500°C. The presence of a liquid phase may be

beneficial if, for instance, one were interested in a high density material, but the possibilities for leakage and chemical incompatibility seem to make such an idea impractical.

B. Composition Selection and Sample Preparation

Compositions for the samples were chosen for varying reasons. The final compositional systems are listed in Table I. The alumina-magnesia systems are the cheapest and most refractory, easy to process and easy to fire. The alumina-titania system has been proposed as a thermal stress damage resistant system[21] due to high parameters of shock resistance (Equations 1-3) and low, even negative, thermal expansion coefficients. Titania-3%silica samples were fabricated because their relatively low thermal expansion coefficients made them a worthy representative type of a high R material[22] (See Appendix B).

The addition of PVA, as previously noted, was designed to increase the porosity of the system via vaporization of the PVA, and to blunt cracks in the bricks. Such particles were obtained in sizes up to 100 microns and ground by ablative action in a Trost Mill.

Each batch consisted of a combination of the particular components, with the total weight being 1500 grams per batch. These batches were mixed and ground in a jar mill with an alumina pebble charge. Where possible, the systems were ground dry for twenty-four hours. In cases where sticking and caking to the sides of the jars occurred, wet mixing with acetone was employed,

TABLE I

Compositions and Firing Times

Batch Number	Forming Pressure (psi)	Al_2O_3 (%)	TiO_2 (%)	MgO (%)	SiO_2 (%)	PVA (%)	Firing Time (hrs)	Temperature (°C)
2	13000	40	45	3.5	9.0	2.5	4	1420
3	13000	40	45	2.5	7.5	5.0	4.5	1420
4	13000	40	45	2.5	7.5	5.0	4	1420
5	8000	45	45	3.5	4.0	2.5	4	1420
8	8000	45	45	3.5	1.5	5.0	4	1420
9	8000	0	94.5	0.5	2.5	2.5	5	1520
10	5000	0	94.5	0.5	2.5	2.5	5	1520
11	8000	88.5	0	6.5	0	5.0	4	1600
12	8000	88.5	0	6.5	0	5.0	4	1600
23	8000	40	45	3.5	9.0	2.5	2	1350
24	8000	40	45	3.5	9.0	2.5	5	1350
25	5000	40	45	2.5	7.5	5.0	5	1420
26	5000	40	45	2.5	7.5	5.0	4	1420
27*	5000	0	92	0.5	2.5	5.0	5	1520
28*	5000	0	92	0.5	2.5	5.0	10	1520
32*	5000	45	45	3.5	4.0	2.5	4	1420
33*	5000	45	45	3.5	4.0	2.5	4	1420

*denotes wet-ground batches

with longer grind-times (forty-eight hours).

A carbowaxing procedure followed the dry grinding (or was combined with the wet grinding process), acetone being the solvent. The mix was dried thoroughly and samples were then "one-way" pressed to form a brick of cross section 2"X4" (Figure 4). Pressing stresses of 5000-13,000 psi (for one minute) were used. The green specimens generally measured 1"-1 1/4" thick. Four to five samples were pressed from each batch.

All samples were low-fired to 1100°C for two hours, with holding times at 200°C and 500°C to allow safe and complete vaporization of the carbowax and polyvinyl alcohol additions. They were furnace-cooled and then high-fired to specifically prescribed temperatures (see Table I) for desired holding times.

C. Testing

One sample brick from each batch was designated as an A sample and tested for flexural strength in three-point bending. A second B brick was notched (Figure 5) and bent at three points for measurement of fracture surface energy, using a method proposed by Nakayama[23] and improved by Tattersall and Tappin[24]. Those samples for which Nakayama's method was unsuccessful were notched as in Figure 6[25] and bent to failure (See Appendix C for analysis) to determine G indirectly. The remaining samples were heated uniformly to 1000°C and repeatedly quenched in ice water (minimum holding time, thirty minutes at 1000°C, five minutes at 0°C). Bricks were periodically removed for examination and

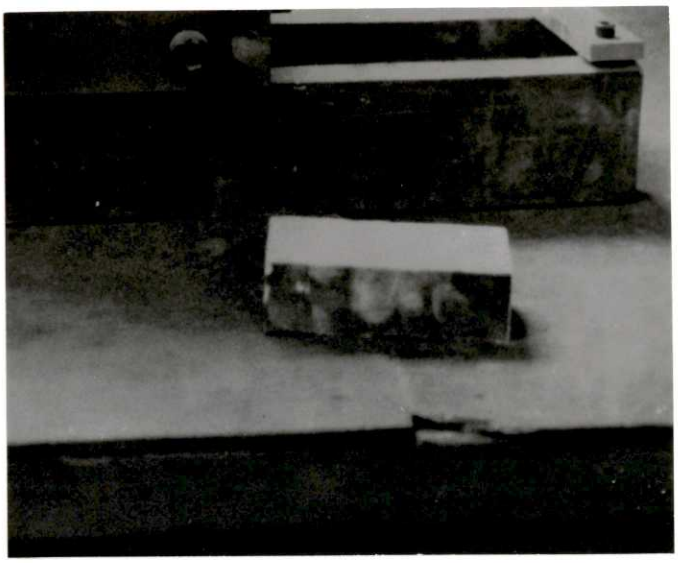

Figure 4. As pressed brick sample.

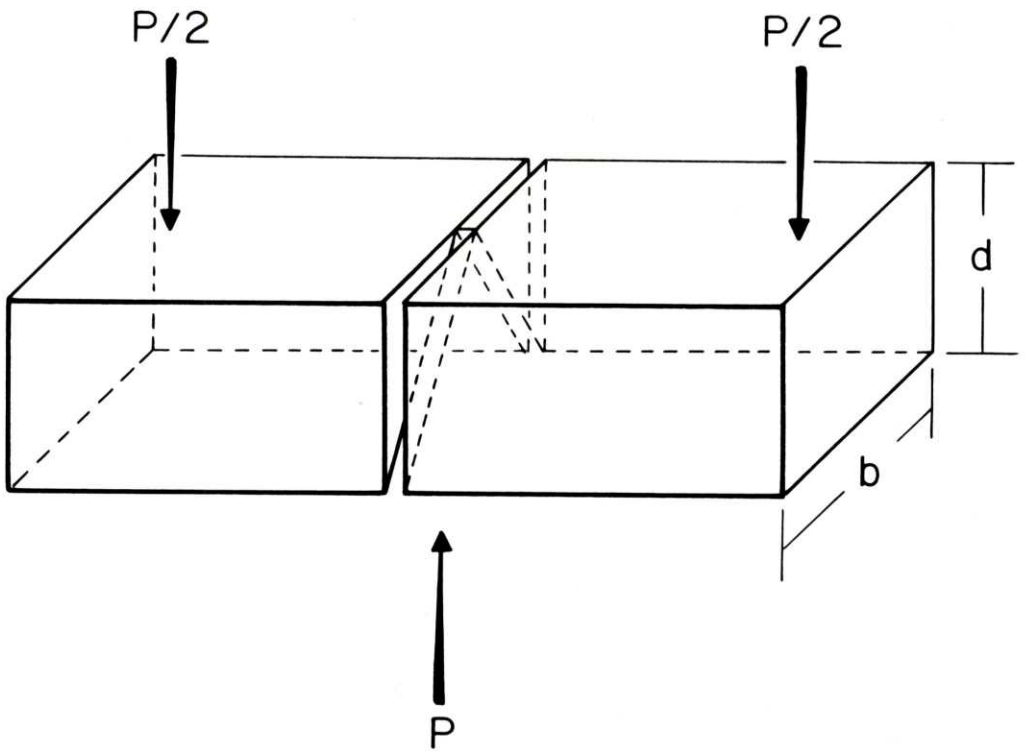

Figure 5. Fracture energy test specimen.[23,24]

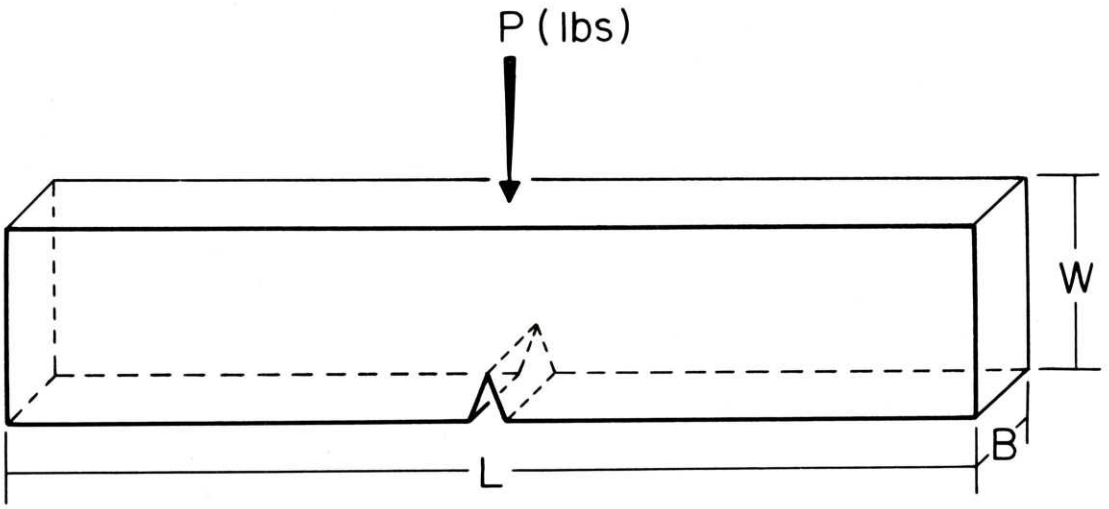

Figure 6. ASTM K_{Ic} test specimen (a = notch depth).[25]

$$K_{Ic} = \frac{6PY}{BW^{1/2}}$$

where $Y = 1.93(a/W)^{1/2} - 3.07(a/W)^{1/2} + 14.5(a/W)^{5/2} - 25.11(a/W)^{7/2} + 25.80(a/W)^{9/2}$.

measurement of crack density on the surface (Surface area per volume and crack length per surface area are determinable from a measurement of cracks per unit length). At some point, those bricks which did no fail were tested in bonding. One inch-square pieces were then cut from all bricks and tested in compression. Chips were taken from both the sample surface and the fracture surface of each brick (separate from the compression samples) and examined further (after etching in boiling phosphoric acid) with the scanning electron microscope.

IV. RESULTS AND DISCUSSION

A. As-Fired Samples

The pressing procedure was the most difficult and variable component of the project. The press and mold used (Figures 7 and 8) prohibited an isostatic fabrication technique and left the as-pressed bricks in a fairly high state of stress (Figure 9)[26]. The effects of these stresses were quite evident in the early stages of sample preparation, as noted by photographs of as-fired bricks (Figure 10). Lowered pressures of fabrication (5000 psi instead of the initial 13,000 psi) and increased binder concentration (6% carbowax 2000 by weight instead of 3% carbowax 4000), substantially improved the appearance of the fired bricks. It is apparent from examination of some sample cross sections (Figure 11) that some imposed stresses were relieved via cracking during the firing stage. However, X-ray analysis (Debye-Scherrer) showed that residual stresses continued to exist (See Appendix D). Surface and interior crack densities are among those listed in Table II.

Scanning electron microscopy was used to examine brick surfaces more closely. Average void sizes in the range of 5-15 microns were determined, the void fraction being about 20% (Table III). Another form of information, number of voids per unit length, has been included as a comparative measure. Comparison of such resultant porosities with injected PVA aggregate particles shows that the different additions, 2.5 or 5% PVA by weight, had no effect on the resultant void fraction of the various systems. This disappointing occurrence may have resulted from the fact that the sintering matrix can close up the voids formed at the much lower

Figure 7. Photograph of hydraulic press (Watson-Stillman, 200,000 lb. maximum load) and slide track (for moving mold back and forth).

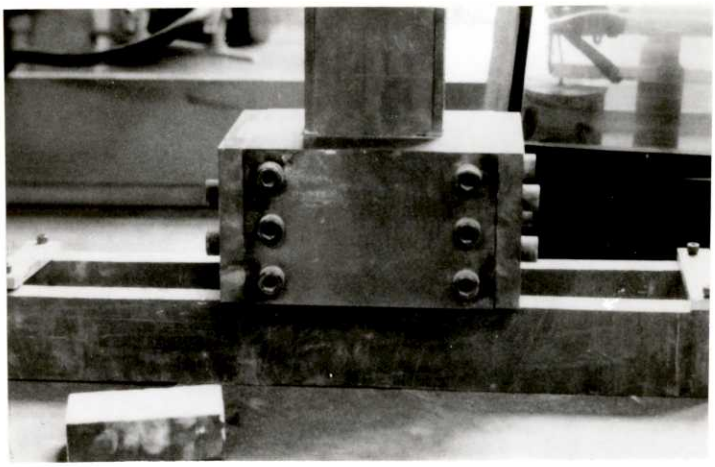

Figure 8. Photograph of mold, slide track, and as-pressed sample.

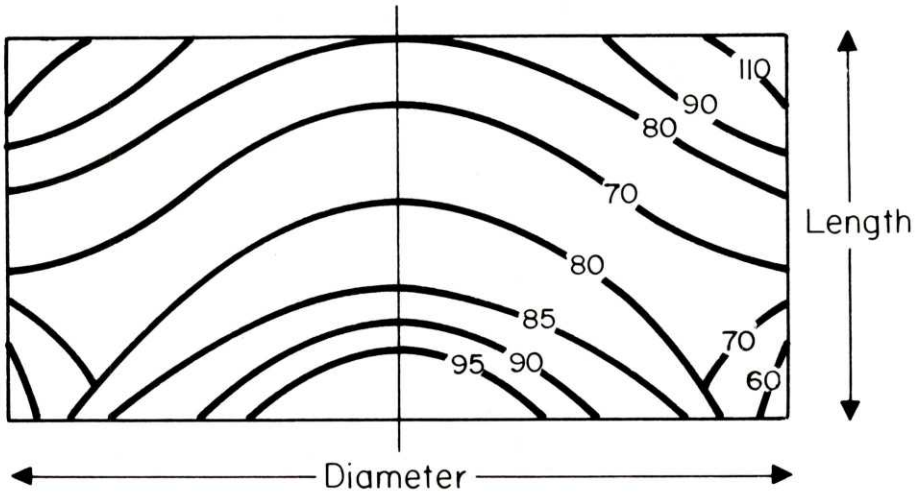

Figure 9. Residual stress contour for "one-way" pressing (L/D = 0.42).[9]

Figure 10. Low magnification SEM photo of as-fired alumina-titania brick (Batch #3, 25X) surface. Cracking during firing is due to relief of residual pressing stresses.

Figure 11. Low magnification photograph of cross section of as-fired, notched-and-bent alumina-titania brick (Batch #3, 1.7X). Note extensive residual stress cracking and gross inclusions ($TiSiO_4$).

TABLE II

Crack Densities

A. Number of Cracks per Inch (N_c) for Number of Cycles (N)

Batch Number	N_c /N	N_c /N	N_c /N	N_c /N	$N_{cross\ section}$
2	1.02/0	2.21/6	3.57/10	6.63/15	3.57/0
3	2.21/0	4.93/6	4.95/10	5.1/15	3.57/0
4	2.5/0	5.61/5	5.95/10	6.12/11	
5	2.55/0				
8	3.06/0	5.44/5	7.3]/10	8.33/15	2.55/0
9	2.5/0	12/3	13/4		4.62/0
10	2.0/0	10.1/2			
11	2.38/0	6.12/2	7.14/3		
12	2.1/0	6.97/3			
23	3.4/0				
24	2.2]/0	2.48/5	17/10	17.3/15	2.04/0
25	2.38/0	4.42/6	4.93/10	5/15	2.04/0
26	4.25/0	6.29/4	9.35/9	9.52/15	1.02/0
27	1.53/0	5.6/3	6.1/4		
28	6.3/0	9.6/3			
32	1.87/0	4.25/2	10.2/3		0.68/0
33	3.57/0	6.46/5	15.64/10		1.36/0

TABLE II (cont'd)

Crack densities

B. Crack Surface Areas per Sample (Inches^2) for Cycles (N)

Batch Number	S/N	S/N	S/N	S/N	$S_{\text{cross section initial area}}$
2	13.4/0	29/6	56/10	87/15	
3	29/0	65/6	65/10	67/15	46.9/0
4	32.3/0	72.5/5	77/10	79/15	
5	32.1/0				30/0
8	35.2/0	63/5	84/10	96/15	29.3/0
9	20.0/0	80/3	87/4		23.9/0
10	21.8/0	110/2			
11	35.9/0	92.5/2	108/3		
12	32.7/0	108.4/3			
23	36.9/0				
24	26.2/0	88.5/5	202/10	205/15	24.2/0
25	27.3/0	52/6	58.5/10	59.5/15	26.5/0
26	50/0	74/4	111/9	113/15	10.9/0
27	9.3/0	34/3	37/4		42.2/0
28	42/0	64/3			
32	18.4/0	41.8/2	100/3		6.7/0
33	35.1/0	63.5/5	153/10		13.5/0

TABLE III

Porosity

Batch Number	Void Surface Area per Volume (Cm^{-1})	Volume Fraction	Average Void Size (microns)
2	286	0.20	10
3	282	0.23	10
4	285	0.215	7
8	382	0.16	6
11	400	0.23	4
12	555	0.16	5
23	351	0.16	7
24	381	0.20	7
25	415	0.23	10
26	825*	0.20	10
27	234	0.18	10
28	218	0.14	12
32	364	0.19	8
33	350	0.20	12

*denotes difficult measurement

temperature of PVA vaporization.

Grain sizes appeared to be quite small in the alumina-titania systems (Table IV). However, the raggedness of the surfaces (Figure 12) often made this measurement susceptible to error, and should therefore be considered approximate.

The alumina-titania compositional systems were two phase in nature, as determined by the X-ray analyzer. The alumina-titania phase diagram, Figure 13, shows that the compositions chosen are within the two phase Al_2TiO_5 + TiO_2 region, but that the possibility also exists for Al_2O_3 + Al_2TiO_5 to occur, due to nonuniform mixing and incomplete sintering. Debye-Scherrer techniques appeared to show that the system was basically single phase Al_2TiO_5 plus minor amounts of titania-silica and alumina-silica, but examination via the X-ray analyzer clearly indicated that certain portions of the microstructure feature significantly more alumina in titania than other parts. This feature may actually be due to the presence of the TiO_2 + Al_2TiO_5 phases predicted by the phase diagram. Those regions of low alumina content showed some cracking at high magnification (Figure 14) on the flatter, more defined grains. The regions of higher alumina content were more continuous (less shrinkage cracking), and ragged, with poorly defined grain structure (Figure 15).

The structure observed appears to contrast that reported by Hannes[21] where complete reaction occurred to form the Al_2TiO_5. Hannes claimed that complete reaction was essential to produce a promising material for thermal shock resistant purposes.

TABLE IV

Grain Sizes

Batch Number	Grain Size (microns)
A. Alumina-Titania	
2	28
3	12
4	10
8	14
23	7.5
24	Not measureable (>7.5)
25	16
26	19
32	9
33	14
B. Alumina-Magnesia	
11	15
12	8
C. Titania-Silica	
9	24
10	27
27	25
28	46*

*denotes 10 hour sintering time

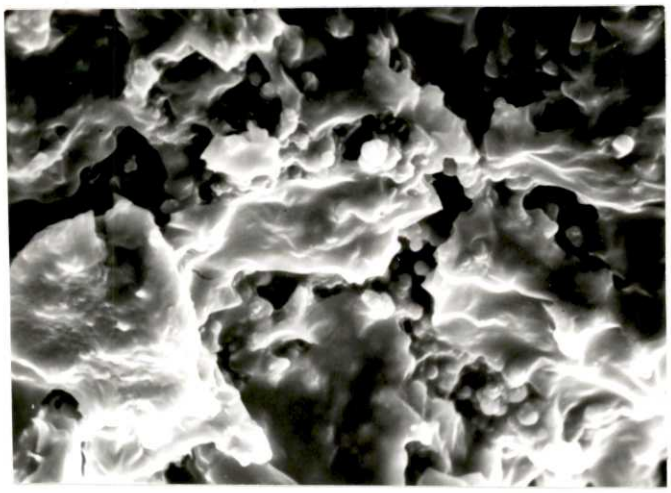

Figure 12 (a). SEM photo of alumina-titania brick surface (Batch #4, 1410X) featuring ragged Al_2TiO_5 grains.

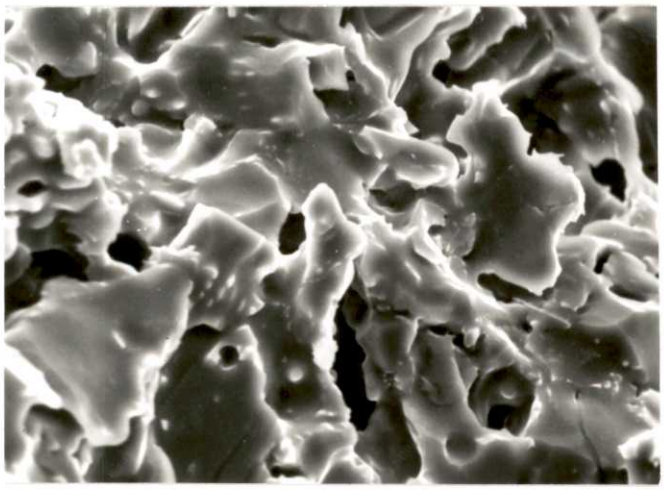

Figure 12 (b). SEM photo of quenched alumina-titania brick surface (Batch #8, 15 cycles, 1200X), where an even more ragged grain structure is apparent.

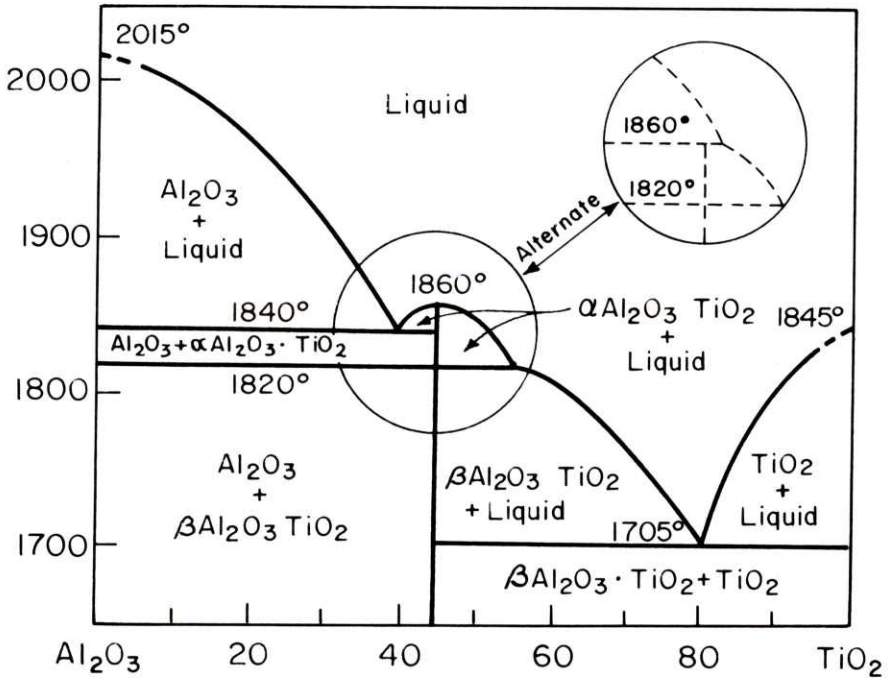

Figure 13. Al_2O_3-TiO_2 phase diagram.[21]

Figure 14. High magnification micrograph of high TiO_2-content phase surface of brick (Batch #8, 12,900X), showing grain boundary cracking in the as-fired material. Some cracking appears to occur along the striations on the surface.

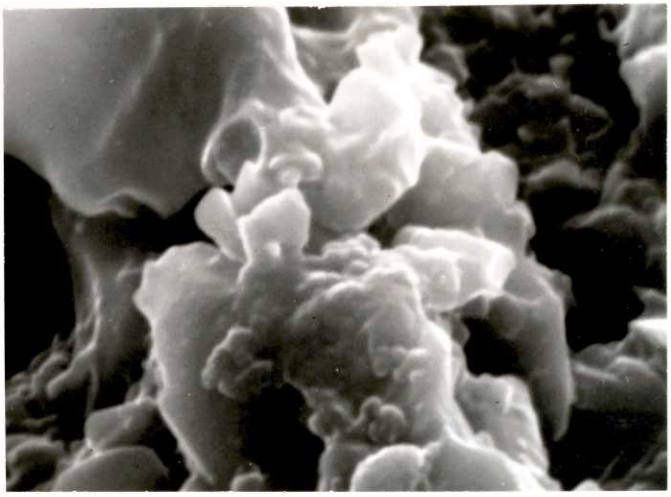

Figure 15. High magnification of Al_2TiO_5 phase ("high alumina content") showing no such cracking as was evident in Figure 14 (Batch #4, 10,000X)

Such a complete reaction as Hannes reports is unusual in such a short heating time (Hannes used two hour sintering times). If the structure analysis of the alumina-titania systems is reliable, then the inference is that yet better properties may be obtained by effecting a complete reaction of the beta-alumina with rutile.

An interesting aspect of the void distribution study was that numerous very small voids often appeared at grain boundaries (Figure 16) in a honeycombed structure. These voids, roughly a micron in size, probably could not have resulted directly from PVA vaporization (due to the overall large sizes of the PVA particles), but may be remnants of closing PVA voids or naturally enclosed by grain growth in the sintering process.

Much of the other discontinuity of the alumina-titania microstructures (Figure 17) is a result of the highly anisotropic thermal expansion characteristics of the principal phase, Al_2TiO_5 (See Appendix D). Note from Figure 17 that, even before the quench cycles, some cracking occurs in the cooling process following the sintering, giving unquenched samples a similar microstructural appearance to quenched samples. Hence these cracks were not necessarily formed during quenching.

Grain size measurements resulted in the calculation of an average grain size in the range of 10-15 microns for the alumina-titania systems (Table IV, note exceptions). The short sintering times are responsible for the small sizes. While such grains generally increase strength, Hasselman's analyses would infer

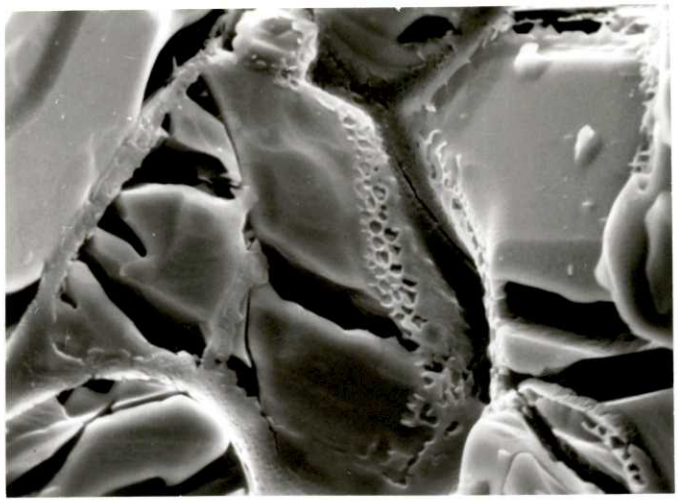

Figure 16. SEM photograph of grain boundary voids in alumina-titania bricks (Batch #2, 1400X), also showing anisotropic shrinkage cracks.

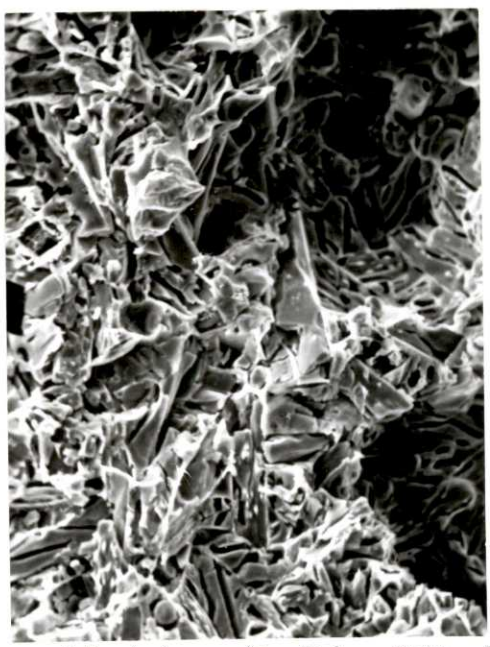

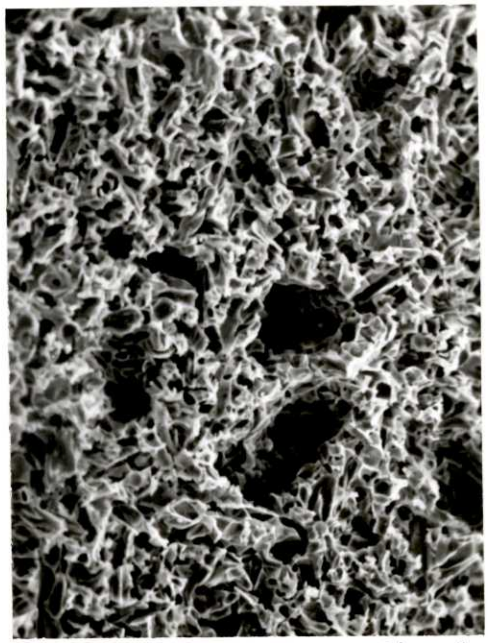

Figure 17 (a). (Left) SEM photograph of surface of as-fired alumina-titania brick (Batch #2, 230X), showing high void content and extensive shrinkage cracking.

Figure 17 (b). (Right) SEM photograph of surface of quenched alumina-titania brick (Batch #2, 15 cycles, 295X), showing that the shrinkage cracking is much more extensive in length but that overall cracking and porosity is not significantly altered.

that larger grains could stabilize longer cracks, to the benefit of the brick exposed to shock conditions.

The titania-3%silica (henceforth called titania-silica) and alumina-9%magnesia (henceforth called alumina-magnesia) systems displayed no anisotropic shrinkage cracking. The former showed quite a definite grain structure (average grain size, 25 microns, note exception in Table IV), with intergranular voids (void size 10 microns, void fraction 14-18%, Figure 18).

A view of the titania-silica grain boundaries (Figure 19) contrasts the shrinkage cracks of alumina-titania with an essentially continuous grain structure. Some stress-induced foldings or facets are also evident.

The alumina-magnesia bricks are fairly porous, with some cracking on the surface of the unquenched bricks (Figure 20). At higher magnification, intragranular porosity and cracking are noticeable in the brick. These cracks are less stable than the flaws in the alumina-titania systems, being both longer, wider and sharper than the cracks in the alumina-titania bricks. This type of cracking appears quite serious compared to the small intergranular defects of the alumina-titania, because of the sharpness and extent of cracking.

The fracture surfaces of the as-fired alumina-magnesia bricks likewise appeared more unstable than those of alumina-titania specimens. Voids which coalesced to form extensive cracks are evident in this system (Figure 21), a much more favorable situation than the catastrophic possibilities of the brick

Figure 18.(a). Titania-3%silica (as-fired) surface (Batch #28, 115X) showing consistent void distribution and (locally) smooth and well defined structure.

Figure 18 (b). Titania-3%silica (as-fired) surface (Batch #27, 630X), featuring intergranular voids and smooth grain structure.

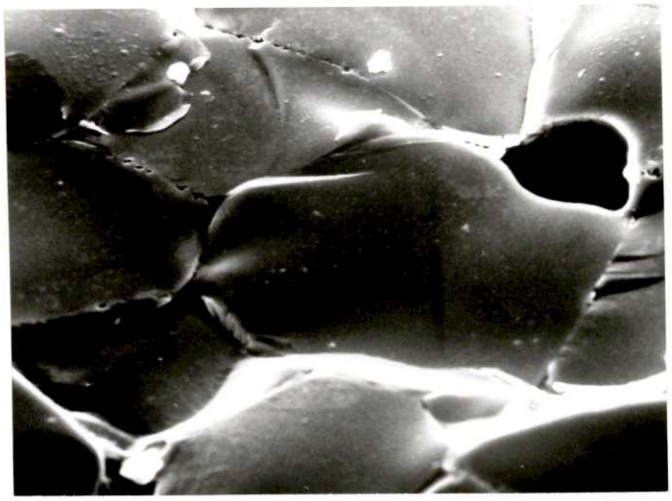

Figure 19. Grain boundary characteristics of titania-3%silica (Batch #28, 1120X), showing folds caused by stress relief during firing. Shrinkage cracking is clearly lacking.

Figure 20. Photo of (as-fired) alumina-9%magnesia brick (Batch #11, 115X), displaying the evident porosity of the sample, and the lack of residual stress cracking.

Figure 21. Evidence of void coalescence to form cracks is shown in this micrograph of alumina-9%magnesia (Batch #11, 580X), on the left and in the upper right-hand corner

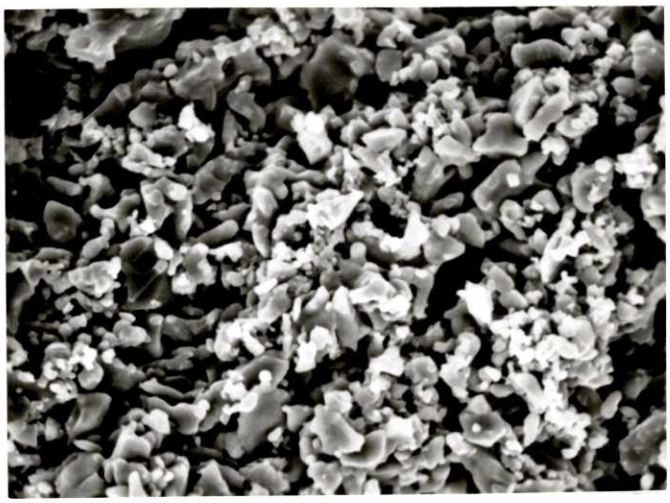

Figure 22. SEM photo of grain structure in alumina-9%magnesia, showing quite small and ragged grains and some void coalescence to cracking (Batch #12, 1175X).

surfaces just observed. The overall porosity, however, is lower than for other systems of similar PVA additions and firing times. Figure 22 also shows that the grains in this mix are fairly small (about 5 microns) and ragged in nature.

B. Quench Surfaces

The most obvious effect of the heat-quench cycles on the bricks was the change in crack density of the surface. The crack densities are often measured as the number of cracks per unit area, or crack length per unit volume. In actuality this is a somewhat difficult measurement for some of the highly damaged bricks. For this reason, point counts of cracks, convertible to a crack area per volume or length per area, have instead been carried out; these are listed in Table II, along with previously noted initial densities. Graphic representation of the number of surface cracks per unit length as a function of the number of cycles is displayed in Figure 23.

These measurements and Figure 23 show that the major portion of the damage by surface cracking occurs in the first few quench cycles in most of the alumina-titania specimens. Certainly the increase in relative surface crack density after the tenth cycle was slight when compared to the value determined at the tenth cycle (with the exception of batch Number 2). Most of these cracks are visible via dye penetrant but are clearly of the microcrack variety, while the few gross cracks appear to emanate from the initial flaws of the as-fired state (Figure 24).

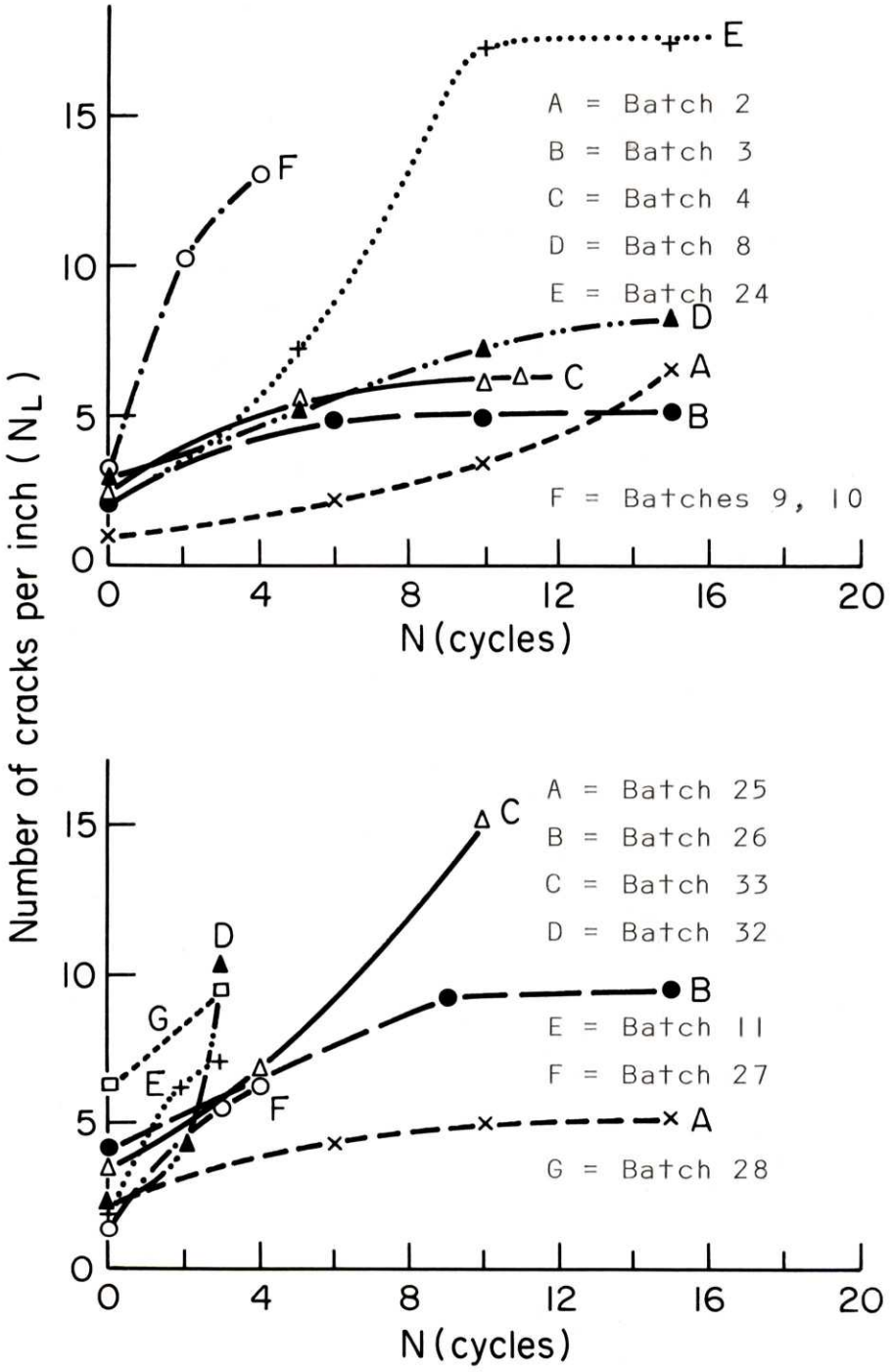

Figure 23. Variation in surface crack density with number of quench cycles.

Figure 24. Photograph of surface (Batch #26, 15 cycles, 1.7X) of quenched alumina-titania brick. Macroscopic cracks are to be distinguished from the faint microscopic cracks. Note that while significant macroscopic cracking appear, those cracks do not run across the dimension of the brick.

Figure 25. Photograph of surface of alumina-titania brick Batch #24, 10 cycles, 1.7X), showing quite extensive micro-cracking.

Figure 26. Another example (Batch #33, 10 cycles, 1.7X) of extensive microcracking (but limited major cracking) in the alumina-titania bricks. Light areas in the picture correspond to regions where more dye penetrant was absorbed by the brick (more porous or more cracking).

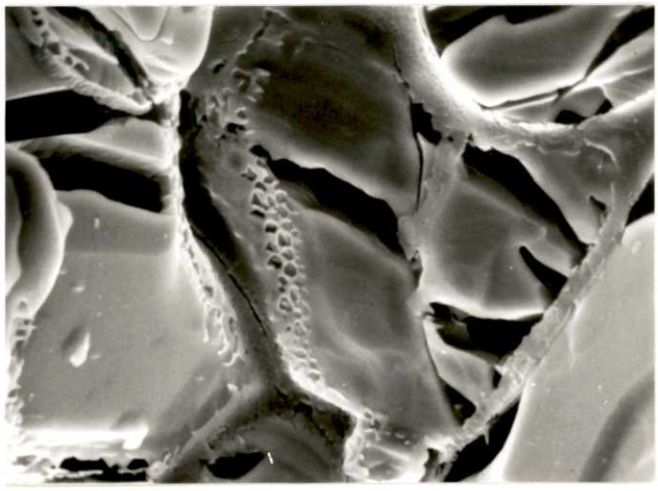

Figure 16. (Repeated) Note that the shrinkage cracks are not sharp-tipped (1400X).

In two cases, surface microcracking was found to be much more extensive (Figures 25, 26) than for the other alumina-titania bricks, although the shape of the N_L vs. N curve in Figure 23 is similar to the other curves. It may be observed in a later section that these systems were initially much stronger than the others.

Study of the fracture surfaces of these quenched samples under scanning electron microscopy was quite beneficial. The anisotropic thermal expansion behavior of the Al_2TiO_5 phase results in further substantial intergranular cracking during the quenches. Anisotropic shrinkage crack densitites of some cycled brick systems may be compared to the same measurements for as-fired systems (Table V).

These shrinkage cracks may be better characterized as planar (two dimensional) voids, since the word crack infers some small radius of curvature at the tips. Figure 16b, at 1400X, shown again for convenience, makes it quite clear that such crack tips do not remotely resemble crack tips of even ductile metals such as aluminum (crack tip radius $\simeq$ 0.5-1.0 microns), but rather occur as naturally blunted flaws about 15 microns in length. These planar voids, therefore, are not much more serious (as stress concentrators) than the more spherical voids closed in during the sintering. Comparisons of the average sizes of these "cracks" in as-fired and quenched bricks do not reveal significant differences, implying that the propagation rate of such cracks is negligible. These shrinkage cracks act as crack

TABLE V

Anisotropic Shrinkage Crack Densities

Batch Number	Number per Inch, As-Fired	Number per Inch, Cycled
2	1980	2100/15
4	1550	2100/11
8	2176	2600/15
24	1995	Not Measureable

Difficulty in measurement of this characteristic prevented more complete data.

arrestors for the brick.

The effects of the assumed residual stresses on the bricks are readily noticed by examination of Figure 27. The cracks shown in Figure 27 follow some of the general contours suggested by Figure 9. A significant number of inclusions also appear on the fracture surface of the titanate bricks. The larger ones are quite easily visible to the unaided eye. These brittle inhomogeneities are mostly $TiSiO_4$ in nature (as determined by the X-Ray analyzer), usually featuring much more titania than silica. Upon closer examination (Figure 28), it is evident that void space of quite significant size surrounds such inclusions, due in large part to variable shrinkage during firing.

The other compositional systems appear somewhat deficient of microcracking. Figure 29 (alumina-magnesia) and Figure 30 (titania-silica), along with Table II, show that extensive macroscopic surface cracking is evident after only a few quench cycles. This inability to deform stably reflects the severe damage each cycle inflicts upon the bricks of these systems. One can certainly presume that such bricks cannot withstand significant further damage, nor could they presently be relied upon to carry any reasonable loads.

The alumina-magnesia bricks featured a quite ragged fracture surface (Figure 31), of fairly uniform composition. There were few cracks or inclusions on the broken surface. Voids were significantly smaller in the alumina-magnesia than in the alumina-titania system (Table III). Residual stress cracking was also

Figure 27. Quite similar to Figure 14, shown here to re-emphasize the inhomogeneous character of the interior of the bricks formed at the higher pressures and with less binder.

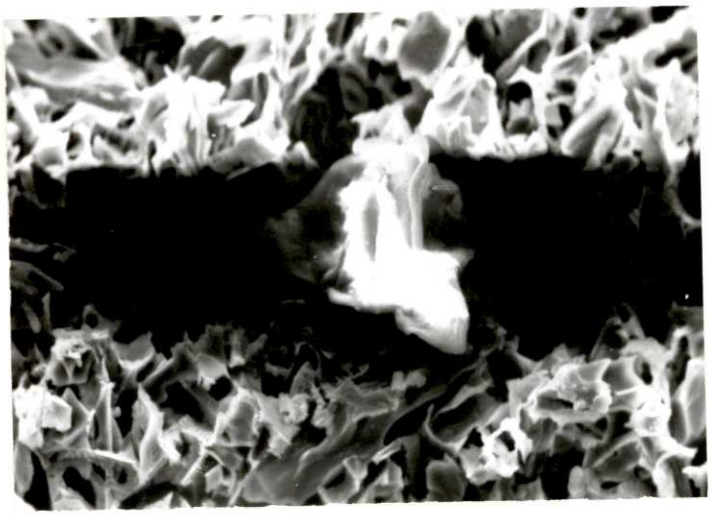

Figure 28. Micrograph of the region surrounding a $TiSiO_4$ inclusion in the alumina-titania bricks (Batch #2, 575X). Note extended void space (as-fired condition).

Figure 29. Photograph of alumina-9%magnesia brick quenched three times (Batch #12, 1.7X), where crack opening (characteristic of macrocracking) is noticeable in most of the flaws on this surface. Very little microcracking is evident.

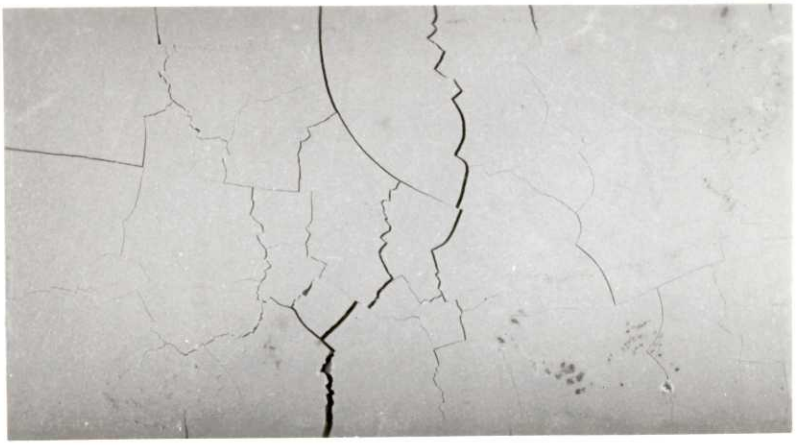

Figure 30. Gross cracking in titania-3%silica photograph above (Batch #28, 3 cycles, 1.7X), again, showing extensive macrocracking and a limited number of microcracks.

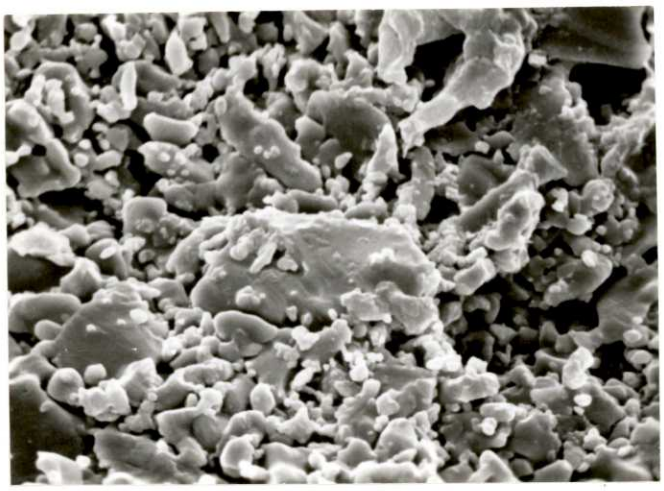

Figure 31. SEM of quenched alumina-9%magnesia brick (Batch #11, 3 cycles, 1200X), showing general raggedness of grains throughout.

Figure 32. Cross section of titania-3%silica (Batch #10, 1.7X), showing some significant residual stress cracking but an otherwise continuous structure.

less extensive.

The fracture surfaces of the titania-silica samples were quite uniform and not far different from the as-fired bricks. Some "press-induced" cracking was evident (Figure 32), but the surface was other wise flaw free and (macroscopically) void free. Although not flat, the entire surface was much more planar than the other samples. Under closer observation, voids were found, nearly all such deficiencies being present at grain boundaries, and of average size 10 microns (Figure 33). They appear much more isolated than those of the alumina-titania system, since the titania-silica grain structure is well defined and more continuous than the alumina-titania system. The continuity accounts for the aforementioned inability to accomodate thermal expansion and contractions without inducing significant stresses.

C. Mechanical Testing

The effect of thermal shock on material strength as noted by previous investigators was primarily recorder for one-cycle tests. While the variation of strength with increased cycling can be inferred, little data has been presented concerning the details of this variation. Table VI shows how the bend strengths of the bricks vary with number of cycles of thermal shocking. The dropoff in bend strength with cycling is quite dramatic in most cases (Figure 34), even though the surfaces of the alumina-titania bricks, for instance, do not appear severely damaged

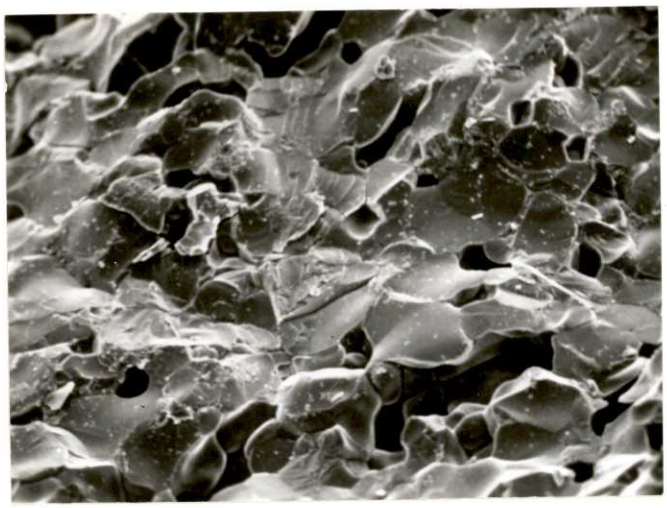

Figure 33. Micrograph of titania-3%silica (Batch #27, 247X), showing general void structure. Compare to Figure 18b.

Figure 35. Photograph of cycled alumina-titania (Batch #26, 9 cycles, 1.7X), showing that the surface has not been significantly damaged in spite of the noted substantial decrease in bend strength.

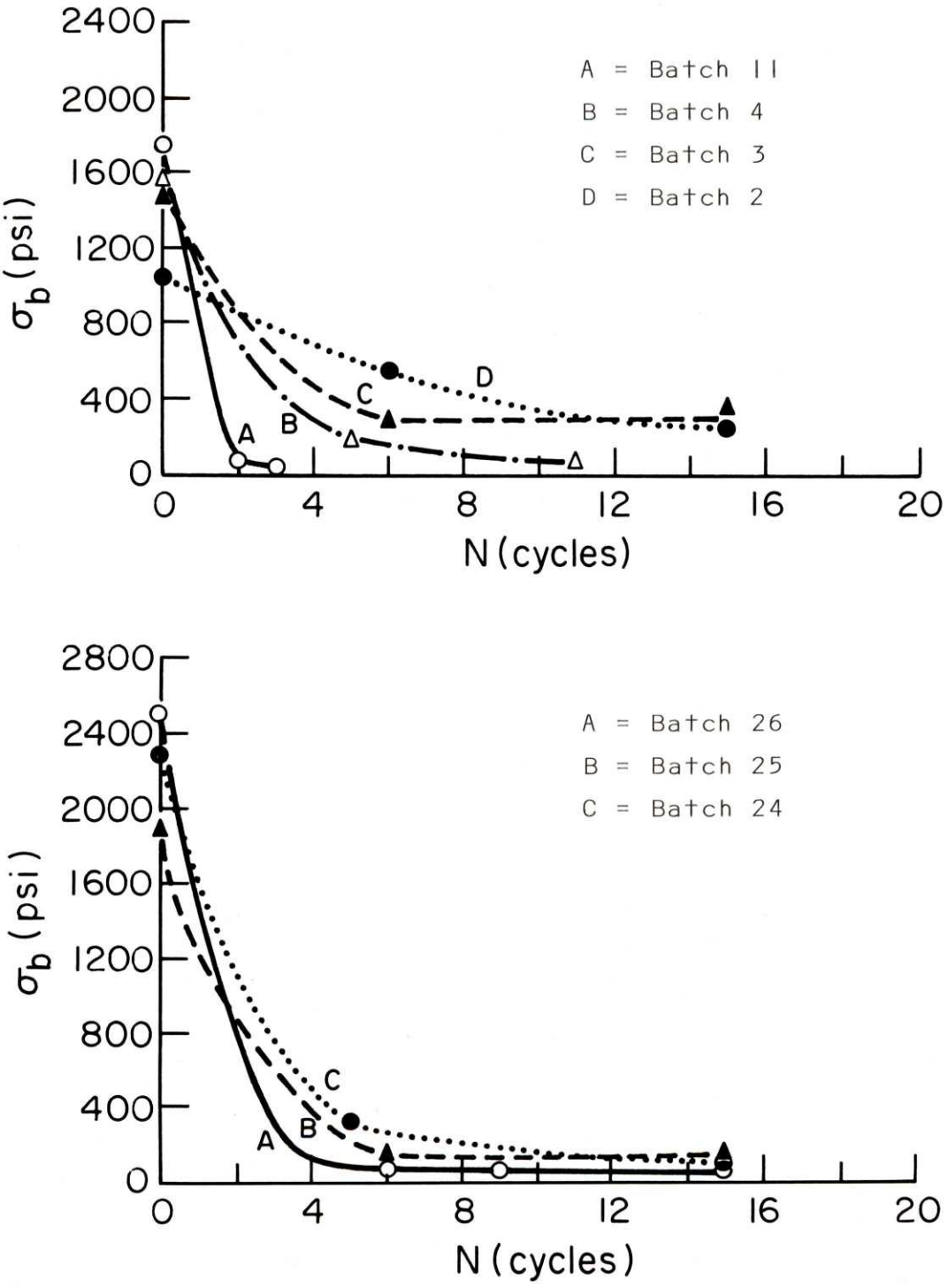

Figure 34. Variation of strength with number of quench cycles (both curves).

TABLE VI

Bend Strengths

Batch Number	σ_b (As-Fired) (psi)	σ_b for N Cycles	σ_b for N Cycles
2	1495	575/6	260/15
3	1455	265/6	350/15
4	1540	195/5	50/11
8	1200	1030/5	105/15
10	4050	65/2	
11	1730	65/2	0/3
23	1460		
24	2600	315/5	115/15
25	1900	140/6	130/15
26	2530	85/4	70/9
27		200/4	
32	2035		
33	1960	135/5	

(Figure 35). Microcracking has occurred, but the brick appears much more structurally reliable than the others. It is seen that the other initially stronger systems, the titania-silica and the alumina-magnesia systems, were the ones most severely damaged by the quench cycling.

Brief investigation of the effect of porous fraction of the alumina-titania bricks on strength failed to show any real dependence of strength on porous fraction. This may have been caused by the presence of critical-sized defects in some bricks or the irregularities of the mixing procedure during sample preparation. Also, the quantity of anisotropic shrinkage, not initially included in the porous fraction, may be an important factor. At any rate, neither volume fraction nor number of voids per length of brick can be correlated to any void fraction-strength dependence. Void fractions calculated from the ratio of density to theoretical density are likewise inaccurate.

If the volume fraction porosity data is assumed to be similar for most of the systems in Table VII, a general effect of grain size on strength may be inferred. Any definite relationship based on such a small sample lot would, however, be impractical and misleading.

The Young's modulus of the flawed bricks was determined from the flexure tests, using:

$$E = \frac{PL^3}{4bd^3y} \qquad (17)$$

where L is the length between supports, b is the sample width,

TABLE VII

Young's Moduli

Batch Number	$E_{measured}$ (psi)	$\frac{b_2 d_2^3}{b_1 d_1^3}$	Load-Deflection Slope A	Slope B	B A
2	1.19×10^5	0.161	32,000	5,470	0.171
3	1.03×10^5	0.212	27,100	6,150	0.227
4	3.5×10^4	-----	8,400	8,400	1.0
10	8.0×10^4	No yield effect observed			
11	3.68×10^5	0.211	29,500	8,890	0.301
23	6.68×10^5	0.351	28,890	9,600	0.332
24	5.86×10^5	0.307	29,000	8,890	0.306
25	5.68×10^5	0.263	28,310	7,375	0.261
26	7.58×10^5	0.30	31,600	8,910	0.282
32*	6.06×10^5	0.188	16,000	2,900	0.182
33*	6.24×10^5	0.231	11,700	2,360	0.202

*denotes grip slippage during bend tests

d is the sample thickness, and y is the deflection (See Table VII). Known values of Young's modulus of the unflawed alumina-titania would enable an effective void fraction to be determined, but the problems encountered heretofore suggest that such an investigation would be frustrating and fruitless.

In the case of alumina-titania, the flexure tests revealed an extraordinary behavior for a brittle ceramic, that is, the load-deflection curves (e.g. Figure 36) were unusual in that an apparent yield point appears to exist at small deflections, after which substantial deformation occurs at lower load-deflection slopes. This second slope is generally between 1/3 and 1/4 of the initial slope, as related in Table VII. Such behavior was most noticeable in the alumina-titania system and to a lesser extent in the alumina-magnesia system. The titania-silica system exhibited no such "plasticity".

The possible mechanisms for such behavior appear most likely to be: (a) decreased stiffness after small deflections, due to the initial presence of longitudinal (residual stress) cracks in the brick; or (b) reduced stiffness via a metastable crack propagation under the bending conditions. While the first is plausible, evidence for the (related) second possibility has been noted from scanning electron micrographs such as Figure 37. It is evident that, even in the very brittle alumina-magnesia bricks, void coalescence accounts for a stable flaw propagation, and this phenomenon is noticeable to a greater extent in the alumina-titania (Figure 38). Such stable crack propagation would suggest a

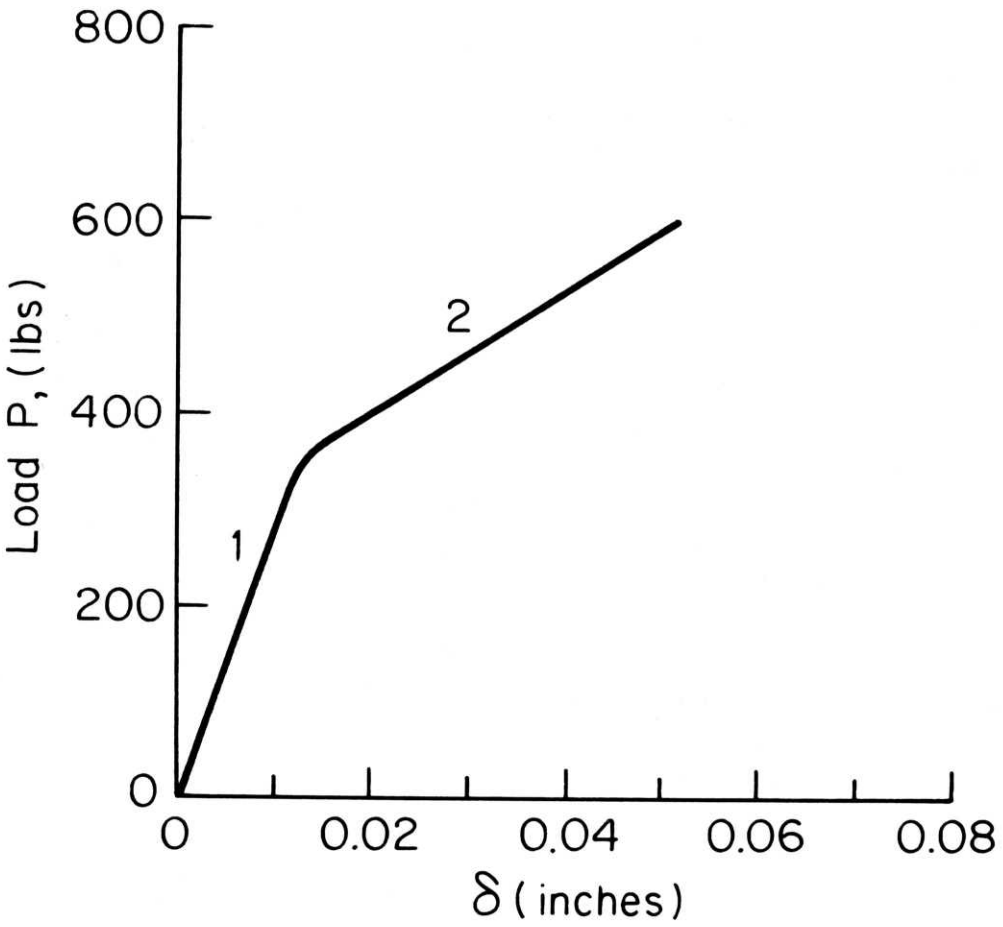

Figure 36. Typical load-deflection curfe for alumina-titania bricks, with primary and secondary slopes noted by (1) and (2), respectively.

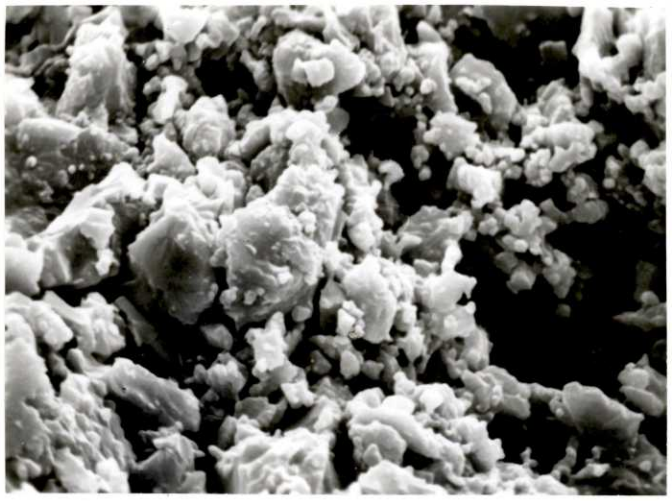

Figure 37. More evidence of void coalescence in cracking of alumina-9%magnesia (Batch #11, 2300X).

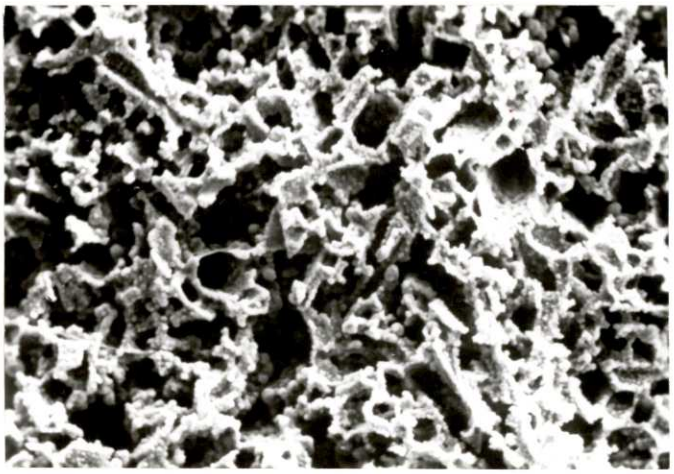

Figure 38. Void coalescence in alumina-titania (Batch #3, 15 cycles, 320X) brick. "Planar voids",i.e. shrinkage cracks, appear to coalesce via short propagation under the existing thermal stress state. The presence of small "beads" on grain surfaces was not expected but may be a result of the quench testing procedure.

relatively high surface fracture energy for the alumina-titania system, a presumption which will later be supported by fracture toughness data and related to this yielding phenomena.

D. Compression Tests

The general loading conditions that refractory bricks encounter require them to withstand moderate applied (static) compressive stresses in addition to surviving adequately both tensile and compressive stresses within the brick. It is evident from examination of the quenched alumina-titania bricks that they appear quite able to withstand many more quenches of severe magnitude before failing. The large number of voids, cracks, and other flaws in the quenched specimens has, however, significantly reduced the tensile strength of the material, to the point where it is useless in tension.

The bricks were broken in compression to check the effect of such shock damage on this material property. The results are shown in Table VIII. The values, although lower than those of polycrystalline ceramics (e.g. Al_2O_3, 30,000-80,000 psi; MgO, 40,000 psi)[27a], are quite reasonable and indicate an ability to withstand moderate loads at elevated temperatures. Nor does it appear that the quenching has seriously altered this property.

E. Fracture Energy Tests

The values of surface fracture energies obtained for the systems tested are listed in Table IX. They are presented for

TABLE VIII

Compressive Strengths

Batch Number	As-Fired σ_c (psi)	σ_c for N_c cycles	σ_c for N_c cycles
2	5000*	9600/6	8680/15
3	6080*	7000/6	6200/15
4	6390	5580/5	5160/11
5	9500		
8		4930/5	4900/15
9	9030		
11	5720	5380/2	
12		880/3	
24	>11,200		
25	4850		
26	11,680	8400/4	4820/20
27	>30,000		
32	>11,200		11,200/3
33	>11,200		

*denotes that the as-fired specimens were tested edgewise to the pressing direction, thus possibly accounting for the strength inconsistency in compression.

TABLE IX

Surface Energies

Batch Number	As-Fired G ($ergs/cm^2$)	G (N cycles)	G (N cycles)
2	7.56×10^4	$2.28 \times 10^5/5$	$7.37 \times 10^4/15$
3	8.12×10^4	$6.5 \times 10^4/6$	$1.07 \times 10^5/15$
4	9.83×10^4	$1.25 \times 10^5/5$	
8	7.59×10^4	$1.07 \times 10^5/5$	
11		$1.44 \times 10^5/2$	
12	3.4×10^4*	$6.23 \times 10^4/3$	
23	7.6×10^4		
24	1.24×10^5	$1.36 \times 10^5/5$	
25	7.16×10^4	$6.38 \times 10^4/5$	
26	1.01×10^5	$6.0 \times 10^4/9$	$4.4 \times 10^4/20$
32	1.5×10^5		
33	1.14×10^5	$4.65 \times 10^4/5$	

* denotes value was determined by ASTM notch test method

(Figure 6)

comparative purposes, since the specimen sizes do not conform to ASTM standards. Table VII shows that the alumina-titania bricks are more resistant to unstable crack propagation than the other systems. Furthermore, although the number of test samples was small, general comparison of the individual compositions is possible. It would seem that higher porosity fractions should reduce fracture energy, but the data are inconclusive about any porosity effects. As discussed earlier, the resultant PVA void size distribution was possibly too broad to avoid serious reduction of other properties than fracture energy. Also mentioned earlier was the fact that voids do appear to stop and/or deter cracks (thus raising G), but the dependence of G upon absolute void fraction cannot presently be determined.

The comparison between such measured fracture energies and the energy required to propagate a single crack through a polycrystalline ceramic ($G \simeq 10^4$ ergs/cm^2) provides favorable information regarding the effects of the minor second phases, voids, and initial flaws. The involvement of more than one crack in eventual material failure is in itself a rewarding accomplishment by the heterogeneities.

The previously discussed plastic behavior of the alumina-titania bricks merits further comment. The apparent explanation is that the stable crack propagation may enable further deflections to occur "after yielding" at lower incremental loads than in the first section of the curve, the overall stiffness of the brick having been reduced by the cracks.

This suggestion is not, however, complete. Difficulty was encountered, for instance, in determining the surface fracture energy of the alumina-magnesia brick by the Nakayama method (Figure 4), due to crack instability. If the cracks in the alumina-magnesia are actually unstable, then the requirement of stable crack propagation as a sufficient criterion does not fully account for the phenomenon.

Values of G, the fracture surface energy were, however, obtainable for several cycled bricks, and are included in Table IX and Figure 39. This G, however, if properly determined, does not change for a particularly fabricated material. Thus this apparent change in value of energy per fracture surface area is due to some effect other than variation in material characteristics.

It would initially be expected that the decreased cross-sectional area of the samples would reduce the energy requisite for failure of the part. This, in fact, has in the past not been found to be the case. Increased cracking out of the general plane of the fracture surface tends to increase the total fracture energy expended en route to failure. Such additional cracking may arise from stress concentrations such as inclusions or residual stresses.

Figure 39, while somewhat limited in data points, implies that the modification of the residual stress state by the added binder and lower fabrication pressures resulted in fewer such initial cracks, while other systems measured an artificial increase in G. Figure 40 (Compare to Figure 27), however, also points out

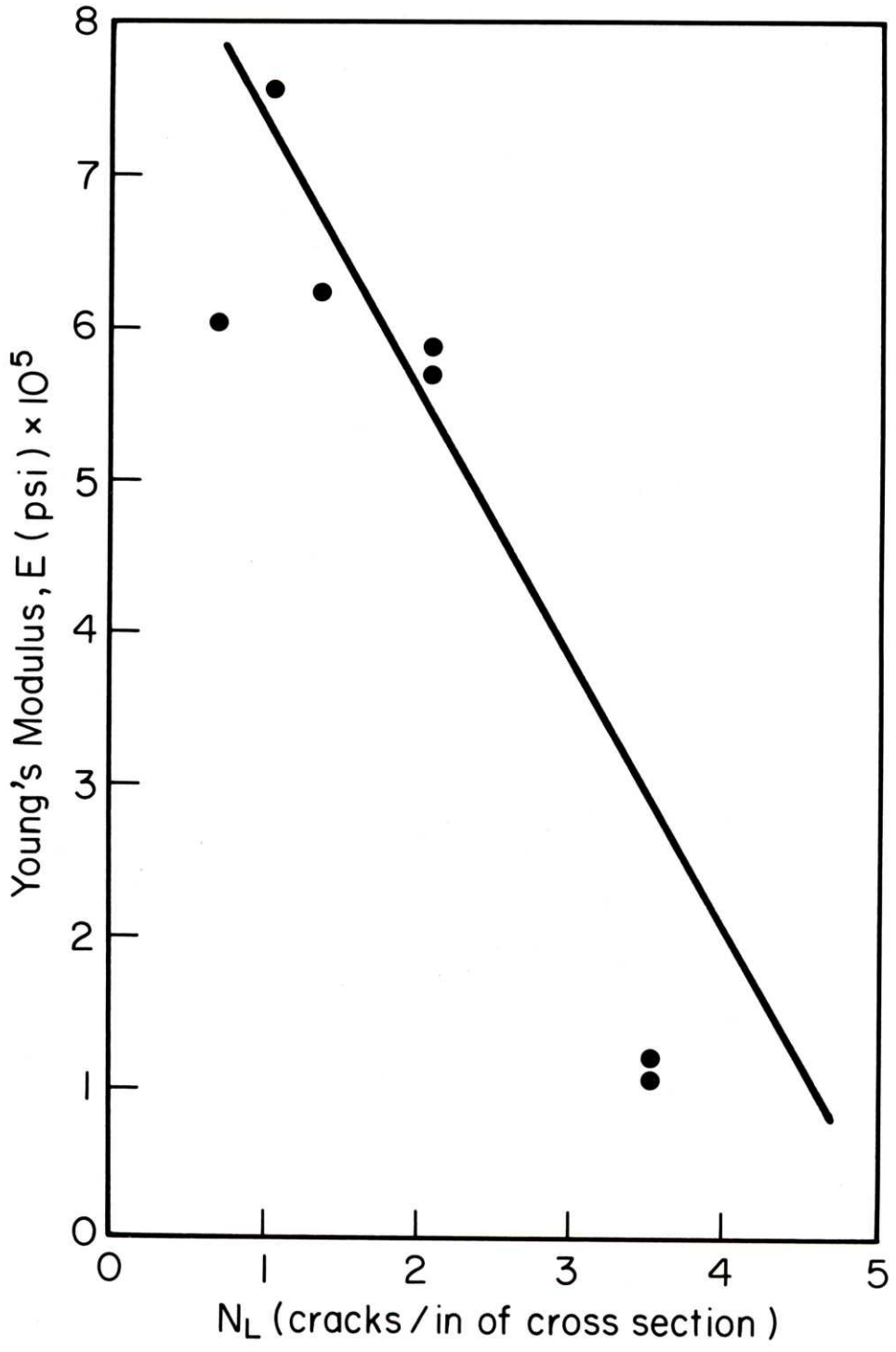

Figure 39. Variation of Young's modulus with initial residual stress crack density.

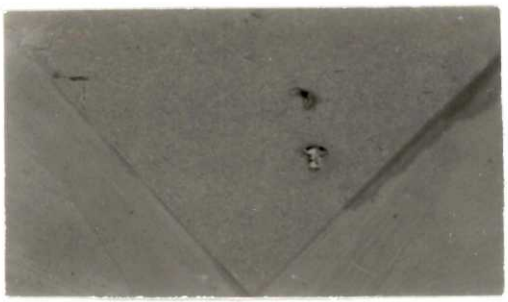

Figure 40. This cross section shows the significant reduction in residual stress cracking and inclusions caused by the lower forming pressures, increased binder content, and wet mixing. Compare this photograph of alumina-titania (Batch #32, 1.7X) to Figure 27.

that the number of gross inclusions appear to have been reduced, possibly by better mixing of the system (Shrinkage cracking, present in both as-fired and quenched bricks, not being significant stress concentrators, have not been considered to decrease the stiffness to the second, lower, value).

Moavenzadeh was able to reduce the measured stable surface energy to a legitimate characteristic value by a quantitative areal analysis of the cracks on the fracture surface of concrete.[28] Although it appears possible in the present case, the difficulty involved in differentiating between shrinkage cracks and flaws otherwise initiated has prevented a good analysis from being carried out. The conclusion, however, must be that G values for cycled specimens are artificially raised by increased areas of cracking.

The relevance of this discussion to the "plastic" effect is that the knee in the load-deflection curve is due to growth of residual stress cracks and flaws initiated at inclusions and inhomogeneities in the material. These flaws (Figure 27) initially reduce the material stiffness, but do not grow (to further reduce stiffness) until a critical stress is applied (the value of which is dependent on the size of the most serious flaw).

While definite quantitative relationships do not exist, it is felt that the residual stress cracks are severe enough (due to their sharp tips) to initiate fracture in the tensile zone of a sample placed in three-point bending. In nearly all brittle systems, however, the initial crack becomes critical and leads

to immediate failure of the specimen, with no evidence of a secondary slope. The shrinkage voids of the alumina-titania specimens, however, appear to blunt such a potentially catastrophic crack and delay its further propagation until the reduced stress state at the crack tip is increased by the shifting of the applied stress state and by some additional loading. The phenomenon of arresting cracks by a form of void coalescence has been discussed previously in another section.

It may be assumed, for purposes of further investigation of this effect, that the secondary slope in the load-deflection plot occurs when some degree of cracking (produced by the first few cracks) is arrested via the method outlined above. Since there were various degrees of residual stress cracking in the bricks, it is likely that this secondary deformation would occur at the load where the stress state near the tip of one of these gross flaws exceeded the theoretical strength of the material. Despite the fact that only one such flaw may actually be necessary, it is logical that the extent of initial cracking should affect the point at which the knee is observed. Table X shows that, in general, the samples with lower residual stress crack surface areas have higher "yield points".

Furthermore, the initial state of cracking does, as implied earlier, affect the Young's modulus of the sample. Figure 41 shows that the specimens with the least amound of residual stress cracking were much stiffer (higher Young's modulus) than those samples where inclusions and gross cracks were in clear evidence

TABLE X

"Yield Stresses" for Alumina-Titania

Batch Number	Yield Stress (psi)
2	950
3	970
4	None
23	1150
24	1050
25	950
26	1110
32	1380
33	1525

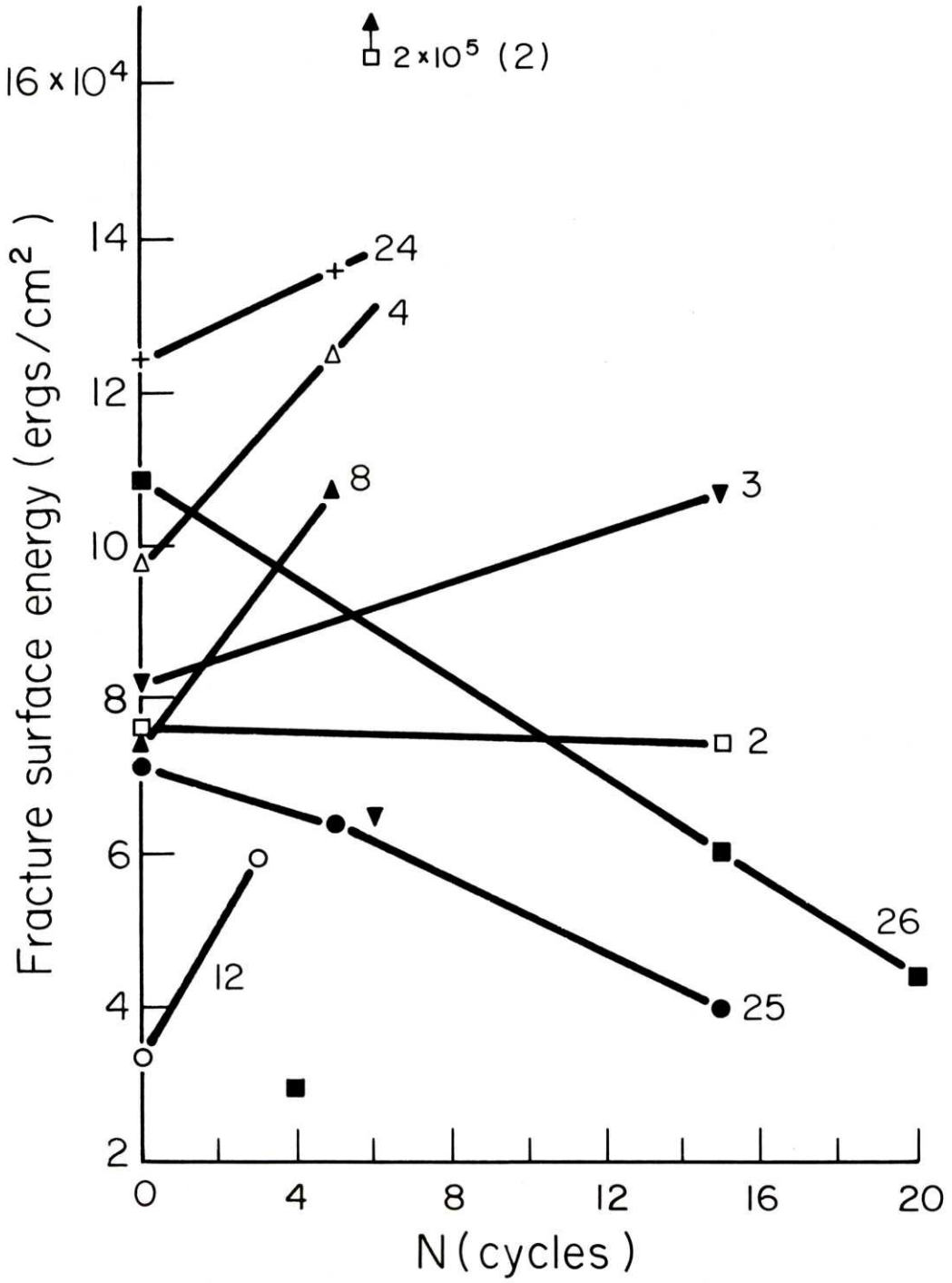

Figure 41. Variation of measured fracture surface energy with number of quench cycles. Numbers refer to batch numbers (See Table IX for fracture energy values).

on the cross section (Compare aforementioned Figures 40 and 27). The quantitative relationship between N_ℓ and E is not clear, but the trend and effects are obvious.

It would next be beneficial to understand how this information relates to the secondary slope of these curves. If a sample were loaded to the point where the slope change occurred, then unloaded and loaded again, the second slope would be proportional to the new modulus. Table VII shows the results where the second slopes were treated as initial slopes in the deflection of a brittle material. The decreased stiffness is due to changes in the parameters used to determine Young's modulus from flexure tests:

$$E_1 = \frac{Pl^3}{4bd^3y} \tag{18}$$

$$\frac{E_2}{E_1} = \frac{P_2 b_1 d_1^{\,3} y_1}{P_1 b_2 d_2^{\,3} y_2} \tag{19}$$

(where E_2 is the secondary modulus) and then the expressions for a "new" $b_2 d_2^{\,3}$ in terms of $b_1 d_1^{\,3}$ for each sample, as in Table VII. This may be viewed as an apparent decrease in cross section dimensions, a result of the overall discontinuities of the cross section. Such a reduction in continuity, without failure, suggests that stable crack growth is occurring. The growth of more such initial cracks should further reduce the secondary slope (as compared to the primary slope of the same material). This has been observed to a general extent (Table VII). The ratio of

secondary to primary load-deflection slopes increases with decreasing residual stress crack surface area. The obvious corollary to this is the fact that the secondary slope is also greater (stiffer) where the residual stress crack area (S_o) is initially small. The cracks may be propagating stably, but fewer of them are, and so the (reduced effective cross section dimensions) gross material is physically more continuous (stiffer) even in the second stage of the bend test.

F. Relevant Parameters and Phenomena in Thermal Shock

The parameters necessary to calculate ΔT_c (Equation 6) for the alumina-magnesia and alumina-titania bricks (values of G, N, and ℓ were not readily measurable for the titania-silica specimens) were determined and used to relate the observed behavior to Hasselman's stability predictions. The ΔT_c's and the various thermal shock parameters were determined and listed in Table XI along with values of the important factors in the expression.

Brief perusal of the two ΔT_c's is sufficient cause for concern. The predicted values are both less than the quench temperatures successfully survived by the brick samples. A direct ΔT_c of 885°C would be expected to result in unstable crack propagation in the alumina-titania. It is possible that the state of stress in the bricks may alter this value ΔT_c from its calculated form, but the initial fact that the surfaces are in tension upon rapid quenching would tend to make the ΔT_c value too high rather than too low. The further evidence that catastrophic failure

occurred in the alumina-magnesia (ΔT_c = 300°C) upon a first cycle of "upquenching" (0-1000°C), where compressive stresses exist on the surface, seems to deviate from the intuitive concept (that compressive stresses would delay fracture), but nonetheless confirms that the state of stress in the body is an important factor to consider in the problem. Hasselman's picture of the ΔT_c's should, if appropriate, correlate with the thermal shock resistance of stress-free bodies.

While Hasselman's analysis appears to be somewhat in error, quantitatively, reasonable qualitative comparison of the thermal shock damage resistance of the systems appeared possible. It was observed that the alumina-magnesia bricks (with the lower ΔT_c) catastrophically failed in the second or third normal quench cycles, that is, after sufficient cracking had occurred at the brick surfaces. These cracks were then able to propagate rapidly through the brick to effect the predicted disastrous fracture. The failure very likely occurs when the surface flaws penetrate beyond a thin surface region and then grow unstably to failure. One-cycle fracture was observed to occur in the case of an unevenly cooled alumina-magnesia brick (immersion of half the hot brick into an ice bath), indicating that catastrophic failure does indeed occur.

Some alumina-titania bricks, however, were quenched fifteen to twenty times and yet did not fail. Significant surface cracking has been observed to occur, giving the bricks ample opportunity to fail due to rapid propagation of a flaw through the

system. Furthermore, an unquenched alumina-titania "upquenched" to 1000°C environment did not fail, as the alumina-magnesia did. Nor were unevenly cooled bricks any less stable than the other quenched alumina-titania samples. While different values of ΔT_c could be caused by other realistic values of G, N, and ℓ, it is still reasonable to wonder whether the parameter ΔT_c has adequately described crack stability criteria in a material of this type, where unstable crack growth was not effected.

Since the expression derived by Hasselman was based on Griffith type flaws, one cannot assume that the expression provides a limiting temperature differential for unstable propagation of blunted flaws. This, in part, is why the expression for ΔT_c does not accurately describe the behavior of the alumina-titania bricks. Furthermore, comparison of the difference in surface fracture energies is not a proper approach in the attempt to rationalize the difference in behavior (from prediction), since the energy of fracture has been included in Hasselman's analysis.

It is quite likely that this situation of non-critical cracks in a brittle material is the major cause of the stability of the system. The surface cracks do not extend far beyond their surfaces before they are joined to shrinkage "voids" and are temporarily arrested. The further reduced stresses away from the surface make it even more difficult to propagate the crack again. Thus the arresting of cracks is more than likely to occur, and likely to resist unstable propagation in the interior portions of the sample. Determination of a critical temperature difference

for blunted cracks (ΔT_c as a function of crack tip radius) apparently would be significantly more helpful in predicting the behavior of systems such as alumina-titania.

The other mentioned factor, the stress state of the brick at the time of the quench, would appear to affect the formation of cracks in the interior of the sample. It is possible that the surface cracks formed in the "tensile zone" upon cooling are stabilized by the reduced level of stress at some point within the sample. Subsequent cycling need not worsen this state unless the surface cracks are wide enough to permit the crack surfaces to cool along with the brick surface (thus creating more tensile-stressed-surface and more cracking). This appears to be another mechanism for raising the resistance to fracture of a thermally shocked brick.

The R-R"' parameters determined by substitution of experimental values into Equations (1-3) are not sufficently meaningful to warrant serious consideration.[29] Values of strength and modulus were extremely low, considering that the bricks tested were in the as-fired state. Values obtained in the project gave parameters for alumina-magnesia and alumina-titania which are not significantly different from each other. More realistic values than σ_b = 2,000 psi and E = 10^5 psi (alumina magnesia) would be σ_b = 20,000 psi and E = $2X10^5$ psi for the 80% dense material. Parameters are also included in Table XI for this case. Typical bend strengths for the alumina-titania are not far removed from measured values (3,000-11,000 psi), but a modulus has not been

TABLE XI

Values and Parameters for Thermal Shock Design

Alumina-Titania

$G = 10^5$ ergs/cm^2

$N = 2\times10^5$ cracks/cm^2

$E_o = 2\times10^7$ psi

$\alpha = 5\times10^{-6}$ in/in-°C (averaged)

$\sigma_b = 2000$ psi

$\ell = 0.0015$ cm

$\nu = 0.25$

$\kappa = 0.0207$ cm^2/sec

Alumina-Magnesia

$G = 3.4\times10^4$ ergs/cm^2

$N = 2.7\times10^4$ cracks/cm^2

$E_o = 3.5\times10^7$ psi

$\alpha = 5\times10^{-6}$ in/in-°C

$\sigma_b = 2000$ psi

$\ell = 0.01$ cm

$\nu = 0.25$

$\kappa = 0.0231$ cm^2/sec

	Alumina-Titania			Alumina-Magnesia		
	I-A	I-B	II-A	II-B	II-C	II-D
R	428	450	3000	171	450	300
R'	5.3	5.4	60	3.42	9.0	6.0
R"	8.85	9.62	69	3.96	10.4	6.94
R"'	3.3×10^{-6}	5.8×10^{-7}	4.78×10^{-7}	4.2×10^{-7}	3.2×10^{-6}	3.6×10^{-6}
R""	0.33	0.058	0.0164	0.0144	0.109	0.122

$\Delta T_{c_{\text{alumina-titania}}} = 885$°C

$\Delta T_{c_{\text{alumina-magnesia}}} = 308$°C

where I-A and II-A are the parameters evaluated for experimentally determined values for alumina-titania and alumina-magnesia, respectively, I-B and II-B represent values for the parameters, evaluated from typical materials properties, and II-C and II-D are values for the parameters, assuming that the bend strength experimentally determined was 0.3% and 0.2% of the actual Young's Modulus, respectively.

TABLE XII

A. Half Cycle Values

time (seconds)	$T_{center\ of\ brick}$	$T_{average\ in\ brick}$	T_{air}	ΔT	σ_{brick} (psi)
120	1360°C	1080°C	800°C	180°C	9.6×10^4
240	1150°C	1010°C	800°C	140°C	7.47×10^4
360	1055°C	930°C	800°C	125°C	6.67×10^4
480	950°C	880°C	800°C	70°C	3.73×10^4
660	875°C	840°C	800°C	35°C	1.87×10^4

B. Full Cycle Values

time (seconds)	$T_{average\ half\text{-}cycle}$	$T_{average\ full\text{-}cycle}$	$T_{surface\ full\ cycle}$	ΔT_{max}	σ_{brick} (psi)
120	1080°C	1105°C	1350°C	245°C	1.3×10^5
240	1010°C	1050°C	1265°C	215°C	1.15×10^5
360	930°C	980°C	1120°C	140°C	7.47×10^4
480	880°C	940°C	1050°C	110°C	5.87×10^4
660	840°C	905	950°C	45°C	2.4×10^4

confidently determined, possibly suggesting that it is quite low compared to that of other ceramics. Nevertheless, a typical ceramic modulus has been assumed and used to determine the parameters. The assumption of 0.2% and o.3% total elastic strain was also used to estimate an approximate modulus.

Experimental results (I-A and II-A of Table XI) show the alumina-magnesia to be more resistant to these effects (stress, heat flux, and heat diffusivity) which cause the initiation of fracture. Modification of II-A in the form to II-C is more practical, yet the alumina-magnesia bricks still appear slightly more resistant to initiation of the first crack than does the alumina-titania. However this is not in line with either the results obtained by substituting typical values of σ_b and E or by reducing the elastic strain to 0.2% (II-D) for alumina-magnesia. The thermal properties of the materials are sufficiently similar that it may be assumed that the strength to modulus ratio is responsible for the respective resistances of the materials to crack initiation.

The energy-based parameters proposed by Hasselman to correlate crack growth to material properties have also been estimated. Both the experimental and typical values fo R"' and R"" for the alumina-titania are greater than the same parameters for alumina-magnesia. Fundamentally, these parameters relate stored energy to that necessary for propagating a crack, R"' being the <u>inverse</u> of the amount of energy required for further propagation and R"" reflecting the extent (in distance) of crack growth. The utility

of R"' is that a larger value, corresponding to a smaller amount of required energy, indicates that a crack will move stably at lower energies in the titania-alumina system than in the alumina-magnesia. R"" is the stable growth distance of the crack. The puzzling aspect is that no such extensive cracks were seen on the alumina-titania fracture surfaces, suggesting that the parameter is not applicable to the case of blunted flaws, provided that the relevant property values are accepted as realistic.

For the reason that the values of R"' and R"" do not appear directly applicable, it does not seem worthwhile to judge the predicted relative behavior of these two systems, in the same way that one should not use thermoelastic parameters to evaluate flawed materials. The parameters exist for study, but similar relations for blunted-crack tips would provide better foundation for evaluation.

As had been noticed by Moore and Daniels[30], increasing numbers of surface flaws reduced the effects of individual surface defects. The alumina-titania bricks (and other pressed samples) were abundant with macroscopic surface cracks, but showed far better fracture toughness than the few slip case alumina-titania bricks (stable crack propagation for measurement of G was not possible) and superior thermal shock resistance (no slip cast bricks survived three cycles). It is possible that the additional gross surfaces cancelling stress fields formed by cracking during the firing can further relieve accumulating stresses during subsequent thermal shock.

The extent of these surface cracks has been shown to level off in the samples where enough cycles were possible to permit such a levelling to occur. However, it is realized that the criteria for a fracture-mechanical treatment of failure of the point are not based on surface flaws but interior cracking (propagation of cracks across the entire sample cross section). Nevertheless, even these surface cracks, which generally do not extend more than about 5 mm into the brick, reflect the fracture toughness of the specimens. In samples of know low surface fracture energies, the surface flaws can readily run across the sample, leading to catastrophic failure. The fact that both titania-silica and alumina-magnesia bricks fractured suddenly into numerous small pieces indicates that randomly placed residual stress cracks were not the significant cause of such critical failures. Rather, the inability of the interior material to arrest the surface flaws cuases rapid growth in spite of a much lower temperature gradient (thermal stress state) in the interior than at the surfaces. On the other hand, the cracking on the surface of the alumina-titania bricks does not lead to failure, although the extent of cracking is in some cases greater than in the other two compositions. Thus it is evident that the effect of the surface crack is to provide gross flaws which test the toughness of a material subjected to thermal shock conditions (meanwhile reducing the stiffness just as residual stress cracks altered the load-deflection curves of unquenched specimens). Whether or not the Moore and Daniels observation actually applies

here is not clear. The crack areas do level off with increasing cycling (Figure 42) and this may be due to a "cancellation" of certain stress states, but the effect does not seem to explain the subsequent material behavior under further cycling.

Random orientation of the polycrystalline mixture, as evident in the above micrographs, seems most likely to be an efficient situation. Preferred grain alignment may be adequately damage resistant, but the gaps created between grains would be much more severe and therefore deleterious to mechanical properties.

The heat flow characteristics of the alumina-titania specimens are not significantly different from those of other ceramics. The specimens had a thermal conductivity of 0.012 cal/cm-sec-°C and a heat capacity of 0.20 cal/gm-°C, of the order of most ceramics. Thus it appears that those properties, i.e., decreased stiffness, relatively large values of G, and high crack density, which most affect thermal shock resistance in the cases presently under consideration, are predominantly the effect of anisotropic thermal expansion properties of the system. The shrinkage cracks formed during initial firing appear to be stable while advantageously affecting the aforementioned materials properties.

This phenomenon suggests that the eventual road to material design for thermal shock damage resistance may follow anisotropic thermal expansion behaviors. Such behavior has been noticed in other systems such as magnesia-alumina spinel and magnesium-dititanate. The compatibility of deformation in such polycrystalline

systems resists critical cracking while establishing short, stable (blunt), flaws within the material. For purposes where tensile strength is not of prime concern to the success of the overall system, such materials bear consideratin. Care should be taken, however, to be sure that such flaws are not sufficiently sharp that crack instability becomes possible during thermal shocking.

V. THE THERMAL PROBLEM

The paractical application of thermal shock analysis lies in the heating and cooling cycles of preheaters or furnaces, where the degree of shocking is much less severe. This reduced severity is due to less stringent boundary conditions, and is parametrically expressed in terms of heat transfer coefficients:

$$Q = h(T_{environment} - T_{surface}) \qquad (20)$$

where Q is the heat flux, h is the heat transfer coefficient, and the temperature difference is between the surface and the surrounding medium. This value of h varies with the fluid medium, e.g. h ≃ 500 kcal/m^2-hr-°C for agitated water, h ≃ 20 kcal/m^2-hr-°C for air, etc.[31] Values are not precise but are often useful when compared for two different processes.

The preheater problem has been simplified and analyzed (Appendix F). An array of bricks is used to heat onrushing pressurized air from 800°C to 1500°C, meanwhile cooling to various temperatures along the length of the array. The bricks are then heated by passing (pressurized) exhaust air over the array in a reverse direction. The steady-state thermal variation at any point of the brick is the desired result. This problem is analyzed in the Appendix for a half and a complete cycle.

The results, showing a relative temperature change of about 7°C of the air for each 1°C change in the brick, gives a rough idea of the steady-state temperature variation along the brick

surfaces. In addition, at any point, the difference in temperature (at the end of the designated time) between brick and the immediately surrounding air is expressed (127°C for two-minute heat-up times). This is the temperature variation at the end of the heating (or cooling) periods.

The real desired information is the variation in brick temperature over a single cycle (steady-state), which is not an easily solved problem. Such data is often determined from dimensionless profile charts if certain necessary assumptions are reasonably satisfied, and is outlined in the Appendix.

VI. CONCLUSIONS

The study of the effects of thermal cycling on ceramic materials revealed that thermal shock conditions may be critical where sharp cracks are concerned, but that blunted flaws, whether by the nature of the flaw or by a form of void coalescence, are markedly more resistant to such environments. Residual stress cracks and other such macroscopic defects were shown to affect strength, stiffness, and resistance to thermal shock damage more significantly than blunt-tipped shrinkage cracks in an alumina-titania material system. More typical refractories such as alumina-8%magnesia and titania-3%silica failed much more readily (three to five cycles from 1000°C into an ice bath) than the alumina-titania (up to twenty cycles with no failures and with negligible spalling). The compressive strengths of the quenched bricks (both alumina-titania and alumina-magnesia) were not significantly reduced from the initial strengths, although the tensile strengths were substantially reduced to the point of uselessness.

The alumina-titania was observed to have a significantly larger surface energy of fracture (G) than either the alumina-magnesia or other typical ceramics. This property, along with the ability of shrinkage voids (cracks) to blunt (initially) sharp cracks, while the ratio of the secondary slope of the plot to the initial slope appears to decrease with increasing numbers of gross (sharp) flaws (residual stress cracks) in the brick.

This phenomena bears significant further investigation.

VII. SUGGESTIONS FOR FUTURE WORK

This project has brought to light a multitude of possibilities for further research in the area of thermal shock. The creation of other systems with anisotropic thermal expansion coefficients, or with other means of introducing small initial flaws, would be of significant import. An accompanying stability-instability relationship for blunt crack-tips should be considered to relate to this class of ceramic systems. Various other methods of crack energy absorption, via liquid phases, for instance, could be explored, along with ways of improving the strength of these materials, e.g. refractory metal reinforcements.

The effect of porosity fraction on the damage resistant behavior of alumina-titania was not determined in the present project. However, the effect of the PVA particles on final porosity and thus the shock resistance should be explored under more controlled conditions. A narrower void size distribution is recommended for study, with a small average void size also suggested.

Exploration into the kinetics of the alumina-titania reaction may clear up the mystery to this author concerning the complete reaction of alumina and titania cited by Hannes. Grain size and porosity may also be better understood and controlled in this system with such information.

The microstructural effects on the plasticity of alumina-titania bear consideration. It seems that this plasticity may be related to the stability of the material with respect to thermal

shock. The creation of high-strength thermal shock-resistant materials with both microscopic and macroscopic flaws appears to be a challenge worth further consideration.

The ability to relate the thermal shock data obtained to practical situations requires some relationship between cycles to failure and heat transfer coefficient (h). Such a relationship could easily be pursued and should aid in future design of thermal shock damage resistant materials.

The microscopic aspects of the alumina-titania bricks revealed little else from the fact that blunted shrinkage cracks were quite numerous. The grain size and porosity fraction averages were quite similar for nearly all of the systems examined. Small grain sizes and similar void fractions were also observed in the alumina-magnesia bricks, while slightly more dense and larger grained structures were evident in the titania-silica.

VIII. APPENDICES

APPENDIX A

Hasselman's Maximum-Tensile-Stress and Fracture-Mechanical Thermal-Stress-Resistance Analogy

$$R = \frac{S_t(1-\nu)}{\alpha E}$$

Tensile stress-Thermal Shock Parameter

$$R_{st} = \left(\frac{G}{\alpha^2 E}\right)^{1/2}$$

Fracture-Mechanical Parameter

$$S_t = \left(\frac{2GE}{\pi \ell}\right)^{1/2}$$

Tensile strength of a plate with a single crack of half-length (Griffith).

$$R = \frac{(2GE/\pi\ell)^{1/2}(1-\nu)}{\alpha E}$$

$$R = \left(\frac{G}{\alpha^2 E}\right)^{1/2} \frac{2(1-\nu)}{\pi \ell^{1/2}}$$

$$R = R_{st}\left(\frac{K}{\ell^{1/2}}\right)$$

The availability of design data may thus determine the method of parameter determination. Note that the fracture-mechanical approach accounts for the thermal shock stability of materials with large values of ℓ.

APPENDIX B

Thermal Expansion of Titanium Oxide[22]

$\alpha_{\parallel} = 5.1 \times 10^{-6}$ in/in-°C

$\alpha_{\perp} = 4.8 \times 10^{-6}$ in/in-°C

$\alpha_{avg} = 4.90 \times 10^{-6}$ in/in-°C

as measured from room temperature to 1500°C.

APPENDIX C

Determination of G from Bend Tests

A. From Nakayama[23] and Tattersall and Tappin[24] Approaches (Figure 5):

$$G = \frac{(E/A)(A)}{2A_o}$$ where E/A is the stored energy per unit area of chart (Instron testing apparatus), A is the area under the curve, and A_o is the fracture surface area. In the testing procedure, crosshead speed of 0.05 in/min and charg speed of 2 in/min at 1000 pounds per full scale give:

$$0.05 \times 2 \times 10 = 2.5 \text{ inch-pounds/inch} = E/A,$$

from which G is readily determined for cases in which stable crack growth was observed.

B. From ASTM testing procedure[25] (Figure 6):

$$K = \frac{6YP}{BW^{1/2}}$$ where P is the applied load at failure, B is the sample width and W the sample thickness.

$$Y = 1.93(a/W)^{1/2} - 3.07(a/W)^{3/2} + 14.53(a/W)^{5/2} + 25.11(a/W)^{7/2} + 25.80(a/W)^{9/2}$$

where a is the notch depth. A value for G_{1c} may be obtained from:

$$K_{1c} = \sqrt{G_{1c}E}$$

and

$$G = G_{1c}/2 \ .$$

APPENDIX D

Debye-Scherrer Results, Comparison to Al_2TiO_5

$d_{Debye-Scherrer}$	I/I_o	$d_{Al_2TiO_5}$ [32]	I/I_o	$d_{Al_2SiO_5}$	I/I_o [33]
4.54	40	4.714			
4.341	40			4.30	25
3.226	60	3.370,3.356	100		
3.146	100	3.169	6	3.18	100
2.546	50	2.654	75		
2.525	50	2.520		2.520	30
2.387	40	2.365,2.357	11	2.355	30
2.339	40	2.320	7	2.350,	30
2.169	50	2.145	20	2.331 2.163	20 20
2.129	40	2.123	25		
1.997	15			2.006	10
1.910	70	1.904,1.900	40		
1.804	70	1.795	52		
1.695	30	1.688,1.685	20		
1.678	10	1.678	5	1.676	10
1.612	40	1.606	20	1.606	3
1.580	40	1.585,1.578	3, 25	1.593	20
1.559	10	1.572,1.551	4, 6		
1.522	10	1.520	6		
1.488	80	1.494,1.487	13, 34	1.475	15
1.452	10	1.481 1.449	36 7		
1.418	5	1.412	3		
1.374	40	1.377,1.372	9, 3	1.377	75
1.326	20	1.369 1.329	7 6		
1.307	40	1.305	21		
1.279	5	1.274	6		
1.267	10	1.266	8		
1.252	15	1.251	14		
1.221	15	1.220,1.218	9		
1.199	15	1.197	14		

APPENDIX E

Thermal Expansion Coefficients for Rutile and Aluminum-Titanate

A. Rutile[34]

$\alpha_{\parallel}$ to c-axis = $(8.816 \times 10^{-6} + 3.653 \times 10^{-9} T + 6.329 \times 10^{-12} T^2$ in/in-°C

$\alpha_{\perp}$ to c-axis = $(7.249 \times 10^{-6} + 2.198 \times 10^{-9} T + 1.298 \times 10^{-12} T^2)$ in/in-°C

as measured from 28°C to 712°C.

B. Aluminum-Titanate[27]

$\alpha_a = 11.8 \times 10^{-6}$ in/in-°C

$\alpha_b = 19.4 \times 10^{-6}$ in/in-°C

$\alpha_c = -2.6 \times 10^{-6}$ in/in-°C

average values, measured from 20°C to 1000°C

APPENDIX F

Temperature Distribution and Thermal Stresses in Refractory Brick Preheater: Calculations

Given: $h_{air} = 20$ kcal/m^2-hr-°C

$C_{p_{air}} = 0.171$ kcal/kg-°C

$C_{p_{brick}} = 0.33$ kcal/kg-°C

$\rho_{air} = 1.18 \times 10^{-3}$ g/cm^3

$\rho_{brick} = 3.6$ g/cm^3

Flow Rate (Q) = 700 kg/sec

Pressure (P) = 10 atmospheres

Assumptions

1) Surface controlled cooling and heating,

2) Materials properties independent of temperature within range of consideration,

3) Constant heat diffusivity,

4) All surfaces exposed to passing air,

5) Air as an ideal gas,

6) All air heated/cooled at same rate (boundary layer heating only).

To find the required brick surface area, assuming bricks to be sheets in a rectangular array (length = 7.3 meters, width and height = 5.4 meters):

700 Kg/sec flow rate

At 10 atmospheres pressure, $\rho_{air} = 1.18 \times 10^{-2}$ g/cm^3

Volume of air passing a unit surface per second = 700/1.18 = 60 m^3.

V_{box} = 5.4x5.4x7.3 =

$\Delta V = V_{total,\ brick}$ =

For bricks of thickness = 5 cm, with dimensions 7.3x5.4 meters, about 300 layers are required to occupy the specified volume. This gives a surface area of 1.2×10^4 m^2 (neglecting thin faces).

Combining,

$$\Delta T_{brick} = \frac{(700\ kg/sec)(0.171\ kcal/kg\text{-}°C)(700°C)(1.2 \times 10^2 sec)}{(3.6 \times 10^3 kg/m^3)(0.33\ kcal/kg\text{-}°C)(81 m^3)}$$

according to the equation:

$$Q = mC_{p_{air}} \Delta T_{air} = mC_{p_{brick}} \Delta T_{brick}$$

where all values are known except T_{brick}. Over the length of the cycle, a 700°C change in the air temperature results in

$$T = 105°C$$

Or, generally,

$$\frac{\Delta T_{brick}}{\Delta T_{air}} = \frac{0.15}{1} = 0.0012 \Delta T(t)$$

and this ratio increases with air heating time. Thus it is shown that the overall temperature difference between outlet and inlet air can be used to estimate the change in brick temperature.

To find the end-cycle temperature difference between the air and the brick surface:

$$\frac{T_{mean}}{2} = \frac{(700\ kg/sec)(1.2 \times 10^2 sec)(0.171 kcal/kg\text{-}°C)(700°C)}{(h)(Area_{brick\ surface})}$$

where the heat flow relation at the interface has been used:

$$Q = hA\Delta T/2$$

and set equal to the heat transferred from the air.

Accordingly,

$$\Delta T/2 = 64°C$$

$$\Delta T = 128°C.$$

This is the difference at any point $T_{brick} - T_{air}$ after a complete cycle and is independent of time. Thi is reasonable because at longer cycle times the brick may cool more while heatng the air, but will heat more when the exhaust is passed over it. Use of this information enabled steady-state temperature ranges to be estimated and related thermal stresses to be calculated. These are presented in Table XII. Both half-cycle temperature differences and stresses and complete cycle temperature differences and stresses are included.

APPENDIX G

Cooling Characteristics of Aluminum-Titanate

A hole was drilled into the brick at the center and one-fourth the total thickness from the faces, so that cooling would be one-dimensional. Thermocouples were inserted and the cooling rate from 1000°C (quenched into ice water) was observed. Assuming a heat transfer coefficient of moderate value, the thermal conductivity could be calculated. The thermal conductivity of the aluminum-titanate was observed to be 0.012 cal/cm-sec-°C. Cooling curves are included in Figure 42.

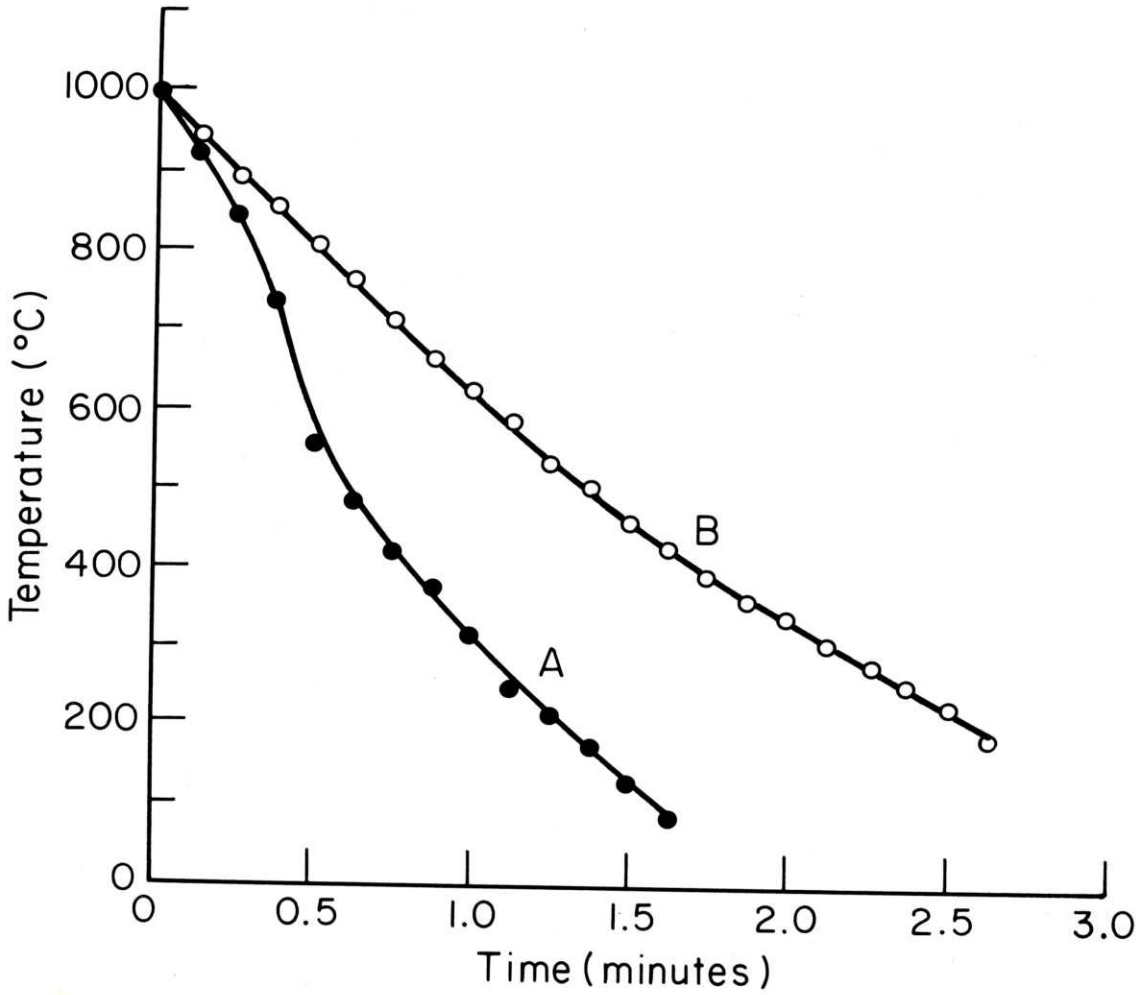

Figure 42. Cooling rates in alumina-titania bricks.
A = Cooling curve at x = 0.6 cm from surface (1/4 thickness from surface).
B = Cooling curve at x = 1.3 cm from surface (center of brick).

IX. REFERENCES

[1] Boley, B.A. and Weiner, J.H., Theory of Thermal Stresses, John Wiley and Sons, New York, 1960.

[2] Hasselman, D.P.H., "Thermal Stress Resistance Parameters for Brittle Refractory Ceramics: A Compendium," Journal of the American Ceramic Society, Volume 49, Number 12, (1967), pp 1033-1037.

[3] Hasselman, D.P.H., "Unified Theory of Thermal Shock Fracture Initiation and Crack Propagation in Brittle Ceramics," Journal of the American Ceramic Society, Volume 52, Number 11, (1970), pp 600-604.

[4] Hasselman, D.P.H., "Elastic Energy at Fracture and Surface Energy as Design Criteria for Thermal Shock," Journal of the American Ceramic Society, Volume 46, Number 11, (1963), pp 535-540.

[5] Berry, J.P., "Some Kinetic Considerations of the Griffith Criterion for Fracture (II)," Journal of the Mechanics and Physics of Solids, Volume 8, Number 3, (1960), pp 207-216.

[6] Schurecht, H.G., "Behavior of Firebrick in Malleable Iron Furnaces," Transactions of American Foundrymen Association, Volume 30, (1922), pp 381-394.

[7] Morgan, W.R., "Thermal Shock Effect on Transverse Strength of Clay Bricks," Journal of the American Ceramic Society, Volume 14, Number 12, (1931), pp 213-223.

[8] Coble, R.L. and Kingery, W.D., "Effect of Porosity on Thermal Stress fracture," Journal of the American Ceramic Society, Volume 38, Number 1, (1955), pp 33-37.

[9] Kingery, W.D. (editor), Ceramic Fabrication Processes, Technology Press and John Wiley and Sons, New York, 1958.

[10] Huang, P.C., "Deterioration of Strength of Brittle-State Porous Bodies," Journal of Applied Mechanics, Volume 32, Number 1, (1965), pp 43-46.

[11] Shaw, R.R. and Uhlmann, D.R., "Effect of Phase Separation on the Properties of Simple Glasses: II. Elastic Properties," Journal of Non-Crystalline Solids, Volume 5, (1971), pp 237-262.

[12] Florence, A.L. and Goodier, J.N., "Thermal Stresses at Spherical Cavities and Circular Holes in Uniform Heat Flow," Journal of Applied Mechanics, Volume 26, Number 2, (1959), pp 293-294.

[13] Mott, N.F., "Brittle Fracture of Mild Steel Plates," Engineering, Volume 164, Number 3374, (1947), p 532.

[14] Hasselman, D.P.H., "Micromechanical Thermal Stresses and Thermal Stress Resistance of Porous Brittle Ceramics," Journal of the American Ceramic Society, Volume 52, Number 4, (1969), pp 215-216.

[15] Hasselman, D.P.H., Gebauer, J., and Krohn, D.A., "Thermal Stress Fracture of a Thermomechanically Strengthened Aluminosilicate Ceramic," Journal of the American Ceramic Society, Volume 55, Number 4, (1972), pp 198-201.

[16] Gupta, T.K., "Strength Degradation and Crack Propagation in Thermally Shocked Al_2O_3," Journal of the American Ceramic Society, Volume 55, Number 5, (1972), pp 249-253.

[17] Hasselman, D.P.H., "Approximate Theory of Thermal Stress Resistance of Brittle Ceramics Involving Creep," Journal of the American Ceramic Society, Volume 50, Number 9, (1967), pp 454-457.

[18] Lynch, J.F., Ruderer, C.G., et.al., Engineering Properties of Ceramics, Published by The American Ceramic Society for Battelle Memorial Institute, Columbus, Ohio, 1966.

[19] Hasselman, D.P.H., "Analogy Between Maximum-Tensile-Stress and Fracture Mechanical Thermal-Stress-Resistance Parameters for Brittle Ceramics," Journal of the American Ceramic Society, Volume 54, Number 4, (1971), p 219.

[20] The polyvinyl alcohol particles were purchased from Air Products, Incorporated, Wayne, Pennsylvania.

[21] Hannes, W., "Aluminum-Titanate as a Temperature Cycle-Resistant Material," Silika Technik, Volume 21, Number 19, (1970), pp 304-306.

[22] Goldsmith, A., Waterman, T.E., and Hirschhorn, H.J., Handbook of Thermophysical Properties of Solid Materials, Volume III, MacMillan Company, New York, 1961.

[23] Nakayama, J., "A Bending Method for Direct Measurement of Fracture Energy of Brittle Materials," Japanese Journal of Applied Mechanics, Volume 3, Number 7, (1964), pp 422-424.

[24] Tattersall, H.G. and Tappin, G., "The Work of Fracture and its Measurement in Metals, Ceramics, and other Materials," Journal of Materials Science, Volume 1, Number 3, (1966), pp 296-301.

[25] Berry, B.W. (editor), Fracture Toughness, Compiled for the Iron and Steel Institute, New York, March, 1968.

[26] Kingery, W.D., Introduction to Ceramics, John Wiley and Sons, New York, 1967.

[27] Lynch, J.F., et. al., Refractory Ceramics for Aerospace: A Materials Selection Handbook, Compiled by Battelle Memorial Institute, Published by The American Ceramic Society, Columbus, Ohio, 1964.

[28] Moavenzadeh, F. and Kuguel, R., "Fracture of Concrete," Journal of Materials, Volume 4, Number 3, (1970), pp 497-519.

[29] Young's modulus reported here was determined by flexure tests and use of Equation (17).

[30] Moore, W.H. and Daniels, R.E., "Fracture Behavior of a Model Brittle Solid Containing Surface Flaws," Journal of the American Ceramic Society, Volume 48, Number 5, (1965), pp 274-275.

[31] Bird, R.B., Stewart, W.E., and Lightfoot, E.N., Transport Phenomena, John Wiley and Sons, New York, 1960.

[32] Holcombe, C.E., and Coffey, A.L., "Calculated X-Ray Powder Diffraction Data for Beta Al_2TiO_5," Journal of the American Ceramic Society, Volume 56, Number 4, (1973), pp 220-221.

[33] Smith, J.V. (editor), X-Ray Powder Data File, Published by the American Society for Testing and Materials, Volume 13, Philadelphia, 1960.

[34] Rao, K.V.K., Naidu, S.V. N., and Iyenger, L., "Thermal Expansion of Rutile and Anatase," Journal of the American Ceramic Society, Volume 53, Number 3, (1970) pp 124-126.